MICROSTRUCTURAL ORIGINS OF VARIABILITY IN THE TENSILE DUCTILITY OF DUAL PHASE STEELS

A Thesis
Presented to
The Academic Faculty

by

Ranbir Singh Jamwal

In Partial Fulfillment
of the Requirements for the Degree
Master of Science in the
School of Materials Science and Engineering

Georgia Institute of Technology
May 2011

MICROSTRUCTURAL ORIGINS OF VARIABILITY IN THE TENSILE DUCTILITY OF DUAL PHASE STEELS

Approved by:

Dr. Arun Gokhale, Advisor
School of Materials Science and Engineering
Georgia Institute of Technology

Dr. Preet Singh
School of Materials Science and Engineering
Georgia Institute of Technology

Dr. Shrikant Bhat
Principal Research Engineer
Automotive Product Applications
ArcelorMittal Global R&D - East Chicago

Date Approved: January 5,2011

This thesis is dedicated to my parents, Mr.Promod Singh Jamwal and Dr.Deepa Jamwal

ACKNOWLEDGEMENTS

I wish to thank my thesis advisor Dr.Arun Gokhale for his constant guidance and support throughout my masters tenure. I thank him for considering me as a potential fit in his lab and finding me worthy enough to handle this research work. His profound knowledge on various metallography and material related issues have indeed helped me broaden my horizon in terms of microstructural analysis and stereology. Along with him I would like to extend my appreciation to Dr.Shrikant Bhat who was heading the project from the Arcelormittal Global R&D side for providing me the steel samples to be investigated. His timely input and suggestions on steel related issues have paid great dividends and helped me immensely in the thesis writing process. Special acknowledgement is given to Dr.Preet Singh for agreeing to be one of the committee members in my thesis defense.

My colleagues have played an integral part in the completion of this thesis. I thank Dr.Yuxiong Mao, Dr.Shenjia Zhang and Ashok Gurumurthy for helping me in many ways in my lab experiments. I was able to learn a lot from the discussions we all used to have in our regular meetings and their inputs on various topics are greatly appreciated. During my research, technical assistance was given by Mr.Gautam Patel whose sound metallography knowledge has helped me greatly to get the desired results.

My stay here in the US during my graduate studies would not have been smooth and pleasant if not for my friends and roommates. I thank Aayush Sharan, Dhaval Kulkarni, Ramasubramni, Pravish Govindan, Priyanka Aggrwal, Ganesh Narayan, Aniruddha Satoskar and Ajay Seshadri with whom I had family away from home.

Last but not the least, my heartfelt gratitude to my parents, Mr.Promod Singh Jamwal and Dr.Deepa Jamwal. This thesis in every respect is dedicated to their unflinching support and love bestowed upon me for all these years especially during this period in Georgia Tech. I also thank my sister Dr.Divya Mehta and my brother-in-law Mr.Ronak Mehta. This thesis work would have not been possible without their support both financially and emotionally.

TABLE OF CONTENTS

LIST OF TABLES

Page

LIST OF FIGURES

Page

SUMMARY

The following research work on cold rolled dual phase steel has been carried out to narrow down on the reasons of variability in the ductility (which is a fracture sensitive mechanical property) of a set of specimens having the same average chemical composition, heat treatment cycle and processing conditions. The prime focus of the experimental work in this regard has been in the area of quantitative fractography using SEM-based and profilometry-based methods. The first order bulk microstructural properties such as volume fraction, surface area per unit volume and spatial distribution of the phases/nature of banding studied through two point correlation function shows little specimen to specimen variation thus eliminating differences in global microstructures as a prominent cause of variability. Global representative microstructures and local microstructures just below the fracture profile have been quantified using stereological techniques to illustrate the influence of the rotations of the ferrite-martensite interfaces which is associated with the tendency to align along the direction of maximum shear stress and in turn decrease the projected area and the extent of ferrite-martensite interfacial fracture. These are the first experimental observations reported for the rotations of ferrite-martensite interfaces due to intense local plastic deformation in dual phase steels and its corresponding influence on a fracture sensitive property like tensile ductility. The quantitative data revealed that the component of the total ferrite-martensite interfacial area per unit volume has a pronounced effect on the interface fracture and consequently on the variability in the tensile ductility as seen comparing the highest and the lowest ductility samples. SEM quantitative study in the present research shows the

influence of number of ferrite-martensite colonies pulled out per unit area of the fracture surface on the tensile ductility, with higher number of these pullouts in the lowest ductility samples. These results do indicate interface fracture due to the incompatible deformation between the two phases as one of the dominant failure mechanisms.

Along with SEM-based quantitative fractography techniques employed for characterization, quantitative fracture profilometry was carried out to determine the extent of fracture path passing through the ferrite and martensite phase. It has been found that the fracture prefers to pass through ferrite where as martensite seems to resist fracture as revealed through the fracture affinity parameter Γ. This is may be attributed to the chemical and the thermo-mechanical processing of these steels, which imparts considerable ductility to the topologically continuous martensitic phase. There is a strong inverse correlation between the fracture through the ferrite-martensite interface and the tensile ductility of the steels studied.

The experimental data clearly shows the variability in the given set of dual phase steels due to local variations in the microstructure occurring in a stochastic manner. To the authors best knowledge such quantitative data on fractography and in-turn delineating the prominent failure mechanism in dual phase steels hasn't been reported before and the results shown provide new quantitative design guidelines in the field of dual phase steels.

CHAPTER I

PROBLEM FORMULATION AND OBJECTIVES

1.1 Problem Formulation

It is the central axiom of materials science that a material's microstructure is governed by its chemistry and processing history, and the microstructure in turn affects its properties and performance. Consequently, quantitative relationships among processing parameters, microstructure, and material properties are of considerable interest in the context of development of robust processing routes that optimize the required material properties. As a result, the scientific literature contains a large number of experimental and theoretical studies on microstructure-properties relationships. However, the majority of these investigations report relationships between *average* microstrucutral parameters and *average* material properties (for example, the dependence of yield stress on average grain size in polycrystalline alloys) [1-4]. On the other hand, some material properties depend on the average microstructural parameters as well as the distributions of microstructural parameters and their extrema. Fracture sensitive mechanical properties such as ductility, ultimate tensile strength, fatigue life, and fracture toughness fall in this category. Development of quantitative relationships between such material properties and microstructural distributions and extrema has received considerably less attention, particularly in the *wrought* metals and alloys. Accordingly, an important objective of this research is to perform a systematic investigation in this direction.

The dependence of the fracture-sensitive mechanical properties on the microstructural distributions and extrema often leads to substantial *variability* in these properties: a set of specimens having the same average chemistry, the same average processing history, and the same average microstructural parameters such as volume fractions of different constituents can exhibit substantially different material properties. For example, Table 1 shows the experimental data on uniaxial tensile ductility (total elongation) of cold-rolled dual phase steel specimens having the same average chemistry and processing history.

Table 1

Room temperature uniaxial yield stress and ductility for cold rolled dual phase steel specimens having the same average composition, processing history, and microstructure.

Specimen Number	Yield Stress (MPa)	Total Elongation (%)
1	701	10.1
2	700	11.9
3	677	13.1
4	663	14.0
5	660	15.8

Note that the ductility (a fracture sensitive property) varies from 10.1% to 15.8% (a variation of more than 50%), although the yield stress (which is not a fracture sensitive property) varies at the most by 7%. Clearly, such variability in the fracture sensitive properties of structural materials such as advanced dual phase steels is not desirable. In the recent years, there have been several studies on the relationships between

microstructure and variability in the ductility and other fracture sensitive properties of *cast* Al-alloys and Mg-alloys, where it has been shown that the variability is related to the presence of processing defects and large pores whose spatial distributions within the cast component vary in a stochastic manner [5,6]. Nevertheless, to the best of the author's knowledge, there have been no investigations to understand the variability in the fracture sensitive mechanical properties of structural *wrought* alloys, particularly of high-strength wrought structural steel products. Consequently, there is a need to develop a thorough understanding of the microstructural origins of the observed variability in the ductility and other fracture sensitive mechanical properties of advanced high-strength structural steels such as dual phase steels. Accordingly, the focus of this research is on stereology and digital-image-analysis-based quantitative microstructural investigation to relate the variability in the microstructure and fracture path to the observed variability in the tensile ductility of a cold rolled continuously annealed dual phase steel. The major objectives and scope of the research are described in the next section.

1.2 Objectives and Scope of the Research

Monotonic and cyclic mechanical properties of dual phase steels have been extensively investigated [7-10]. Classical dual phase steel contains islands of martensite (~ 20-30 volume percentage) distributed in the ferrite matrix. DP 600 is the typical dual phase steel in this category. Most of the earlier investigations on the microstructure-properties relationships in the dual phase steels (i) focus on relationships between the *average* microstructural parameters (for example, volume fractions of martensite and ferrite) and *average* mechanical properties, and (ii) concern the microstructures where ferrite is the

topologically continuous phase (matrix) containing islands (or partially connected regions) of martensite, which typically happens at martensite volume fractions lower than 50%. On the other hand, the present research (i) is concerned with high strength (~ 1000 MPa) high martensite (>50%) dual phase steel where the martensite is a topologically continuous phase (matrix) containing a dispersion of islands of ferrite, and (ii) focuses on understanding the microstructural origins of the *variability* in fracture sensitive mechanical properties, in particular variability in the room temperature uniaxial tensile ductility. The research involves quantitative microstructure characterization using stereology and digital image processing [11-12] and quantitative fractography using scanning electron microscopy (SEM) and fracture profilometry [5,6,13,14,15]. The objectives of the research are achieved through the following tasks.

- Quantitative characterization of the tensile fracture surfaces observed in SEM to quantify the extents of fracture path generated by fracture along the interfaces between martensite and ferrite, fracture mode containing dimples, and fracture generated via pull-out of packets of ferrite-martensite colonies containing several martensite crystals.
- Quantitative fracture profilometry using optical metallography and digital image analysis to estimate the extent of fracture path through ferrite, martensite, and through the interfaces between martensite and ferrite.
- Application of stereological techniques to estimate the interfacial area between ferrite and martensite that is oriented *perpendicular* to the direction of applied tensile stress. This parameter is estimated separately for the local microstructure

just below the fracture profile as well as in the bulk three-dimensional volume away from the fracture surface.

- Application of stereological techniques to estimate volume fractions of ferrite and martensite phases, spacing between the bands, and two-point correlation functions in the bulk microstructures.

To the best of the author's knowledge, these are the first experimental *quantitative* fractographic data on dual phase steels; all the earlier investigations were limited to *qualitative* fractographic observations using SEM. Further, none of the earlier investigations utilized fracture profilometry to quantify the extent of fracture through different constituents. The analysis of the quantitative fractographic and microstructural data obtained in this research leads to useful guidelines for reducing the variability in the tensile ductility of the dual phase steel under investigation.

CHAPTER II

BACKGROUND AND LITERATURE REVIEW

The central objective of this research is to understand the microstructural origins of variability in the tensile ductility of a cold-rolled dual phase steel designed to achieve a tensile strength of 1000 MPa. The variability in the tensile ductility is studied in a set of specimens having the same average alloy chemistry, thermo-mechanical processing history, and heat-treatment. To know the microstructural origins of the observed variability in the tensile ductility in these specimens, it is necessary to develop a thorough understanding of the chemistry, thermo-mechanical processing, microstructure, and physical metallurgy of dual phase steels. These aspects are reviewed in the next section of this chapter. The experimental facets of this research involve applications of stereology and digital image analysis techniques for quantitative microstructure characterization, and quantitative fractographic techniques for quantitative characterization of the tensile fracture surfaces. The subsequent sections of this chapter provide a brief background on these methodologies extensively used in the experimental work reported in the next chapter.

2.1 Dual Phase Steels

Dual phase steels are a category of advanced high strength structural steels (AHSS) where the microstructure is optimized through controlled thermo-mechanical processing as the steel is cooled from the $\alpha + \gamma$ region in the intercritical annealing temperature regime. Depending on the chemistry and thermo-mechanical processing, the AHSS steels may contain ferrite, martensite, bainite, and/or retained austenite. Dual phase steels

contain two major phases, namely, ferrite and martensite (or in some cases, bainite). Dual phase steels were developed in the 1970s; their properties have been substantially improved over the past four decades via better understanding of the physical metallurgy and processing-microstructure-properties relationships. Dual phase steels are extensively used for structural automotive applications.

Most widely used dual phase steels contain 20-30% martensite or bainite dispersed in the topologically continuous soft phase, ferrite (see Figure1).

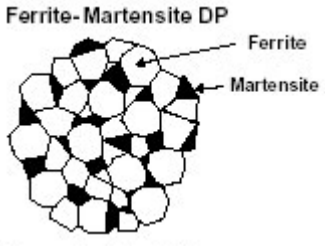

Figure 1: Schematic representation of the microstructure of DP steels.

Due to high topological connectivity of ferrite (a soft and ductile phase), dual phase steels have excellent ductility. In the dual phase steels, the plastic deformation initiates in the ferrite phase and remains concentrated in ferrite, which leads to a high rate of work hardening [16-18]. The high rate of work hardening combined with high ductility gives rise to high ultimate tensile strength (UTS) in the formed components made from dual phase steels as compared to the UTS levels in other high strength steels having comparable yield stress. Therefore, the dual phase steels have a yield stress to UTS ratio [19], which is desirable for components fabricated via metal forming. Further, dual phase steels do not have sharp yield point; rather they exhibit a continuous yielding behavior, which is also beneficial [20]. The low yield stress and continuous yielding behavior of

dual phase steels is attributed to the presence of mobile dislocations generated in ferrite when austenite present in ferrite matrix transforms to martensite under the constrains imposed by the surrounding ferrite (during heat treatment). The dislocations are also generated in ferrite due to the stresses induced by the volume change associated with the austenite to martensite transformation [21,22]. Thus, the optimization of microstructural geometry via appropriate choice of chemistry and thermo-mechanical processing conditions gives rise to a remarkable combination of mechanical properties in the dual phase steels and makes them attractive for numerous structural automotive applications.

2.1.1 Chemistry of Dual Phase Steels

The alloy design of dual phase steels is guided by the following requirements.

1. The ferrite phase in dual phase steels must be soft and ductile. Therefore, an alloying element should not cause substantial solid solution hardening in ferrite.
2. An alloying element must stabilize austenite and promote partitioning of C to austenite so that high strength martensite can be produced upon cooling from the two phase austenite-ferrite region.
3. Since formation of martensite is desired in the dual phase steels, an alloying element should retard the bainite start (B_s) and bainite finish (B_F) temperatures, so that austenite to martensite transformation is promoted.

C, Si, Mn, Cr, Mo, and micro-alloying additions are common alloying elements present in most of the dual phase steels. The role of these alloying elements in controlling the microstructure, properties, and performance is described as follows.

Carbon

In general, dual phase steels fall in the category of low carbon steels, and therefore, contain less than 0.2% C. The low carbon content improves weldability and formability of dual phase steels; the properties that are particularly important for structural automotive applications. The inter-critical annealing temperature is usually selected such that subsequent rapid cooling leads to formation of microstructure with varying amounts of discrete islands of martensite distributed in the matrix of topologically continuous ferrite. It is important to recognize that the strength of the dual phase steel depends on the carbon content of the martensite and the relative amounts of ferrite and martensite in the microstructure. Therefore, the required strength level can be obtained in lower carbon dual phase steels simply by increasing the volume fraction of martensite, which can be achieved by increasing the inter-critical annealing temperature. In such high strength dual phase steels, the martensite volume fraction may be high enough to be the topologically continuous phase in which the regions of ferrite are dispersed. The dual phase steel studied in the present research belongs to this category.

Manganese

Dual phase steels contain 1 to 1.5% Mn. Addition of Mn at these levels imparts sufficient hardenability to austenite for the martensite formation subsequent to inter-critical annealing. The hardenability of austenite is increased because Mn shifts the TTT curve to the right, thereby discouraging ferrite and pearlite formation, which facilitates martensite formation. Figure 2 illustrates the effect of Mn in the processing of dual phase steels.

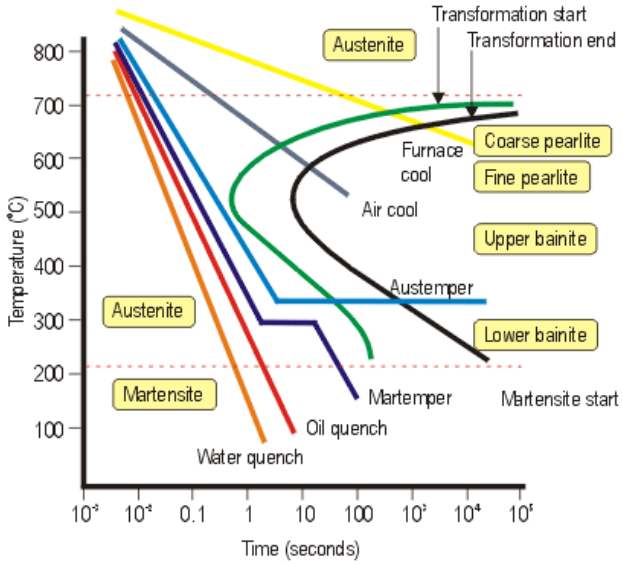

Figure 2: TTT curve showing various cooling rates giving different microstructures.

It is important to point out that a decrease in the carbon content of a steel decreases its hardenability. Therefore, the Mn content of lower carbon dual phase steels is increased to compensate for the decrease in the hardenability resulting from a lower carbon level (for a given cooling rate or if the process is cooling rate limited).

Micro-alloying Elements

Dual phase steels also contain very small amount (s) of intentionally added micro-alloying elements such as V, Ti, and/or Nb. These elements are very strong carbide formers. They form very fine grain boundary carbides that are stable at temperatures of the order of 1200°c. The presence of these carbides on the austenite grain boundaries retards austenite grain growth during the processing steps such as hot-rolling and limits the austenite grain size in the hot-rolled steel, which facilitates formation of fine-grained

ferrite during subsequent inter-critical annealing that produces the dual phase microstructure.

Cr and Mo

Some dual phase steels contain Cr and/Mo alloying additions. These elements shift the TTT curve towards the right, and thereby decrease the critical cooling rate (i.e. the minimum cooling rate to ensure that austenite is converted into martensite during quenching) which in-turn increases the hardenability. In general, the carbon content, nature and amounts of alloying elements, inter-critical annealing temperature, and quench rate subsequent to sub-critical annealing to form martensite affect the mechanical properties of the dual phase steels. Therefore, different combinations of these process variables can be used to achieve the required properties in the processed dual phase steels.

2.1.2 Processing of Dual Phase Steels

Production of dual phase steels involves extensive thermo-mechanical processing. Cast steel billets (typically, ~ 225 mm thickness) are hot-rolled at about 1200°c to reduce the thickness to about 6 mm. Hot-rolling may be carried out in several passes followed by controlled cooling. The hot rolled coils are then cooled to room temperature. Substantial austenite grain growth can occur during hot-rolling as it is carried out at high temperature. Coarse austenite grain size developed during hot rolling can adversely influence the ferrite and martensite grain sizes in the final dual phase microstructure. This is avoided via addition of micro-alloying elements such as V, Ti, and/or Nb. These

elements form very fine carbides on the austenite grain boundaries that are stable at hot-rolling temperature. The carbides retard austenite grain growth during the hot-rolling of the steel billets as discussed in the previous section.

Hot-rolling breaks down the cast steel microstructure and distributes the alloying elements more uniformly via homogenization due to diffusion. Nonetheless, despite substantial homogenization that occurs during hot-rolling process, depending on the steel chemistry, billet casting conditions, and hot-rolling process parameters, some spatial segregation of Mn is present in the steel leading to so called "manganese banding" that can influence the morphological anisotropy and spatial distribution of martensite regions in the final dual phase microstructure. Hot-rolled steel has ferrite-pearlite microstructure. The hot-rolled steel may be cold-rolled to further reduce the thickness (typically < 2mm).

The next step in the processing is inter-critical annealing. For this purpose, the steel is austenitized at a suitable temperature range (750°c to 850°c) and then cooled for inter-critical annealing between A1 and A3 temperature in the austenite-ferrite two phase region. The choice of the inter-critical annealing temperature is dictated by the steel chemistry and the relative amounts of ferrite and martensite desired in the final microstructure. The steel is rapidly cooled from the inter-critical annealing temperature to room temperature at cooling rate of about 1000°c per second by quenching in water. The quench rate is a critical process parameter; the quenching must be such austenite transforms to martensite but not to bainite or pearlite-ferrite phases. The microstructure and strength of the martensite formed also strongly depends on the quench rate. The alloying elements such as Mn, Cr, and Mo lower the quench rate needed to obtain the

required dual phase microstructure after quenching. Figure 3 illustrates combinations of alloy content and cooling rates required to achieve a dual phase microstructure.

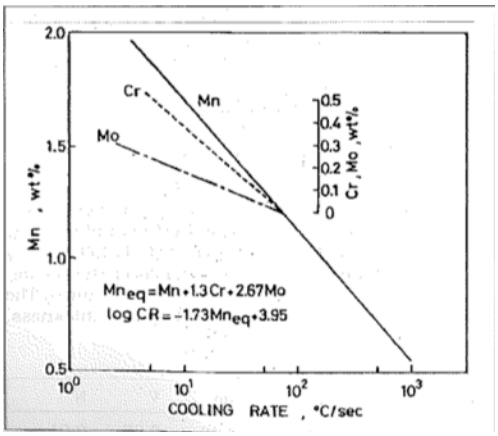

Figure 3: Relationship between alloy content and critical cooling rate required for the formation of dual phase structure. [20]

The tensile strength increases and the total elongation decrease monotonically with an increase in the quench rate. This trend is also obtained with an increase in the alloying element such Mn, Cr and Mo. Therefore, different combinations of the composition and processing conditions can lead to the same set of mechanical properties [20,22,23].

The quenched dual phase steel is tempered at about 200°c to temper the martensite and then air-cooled. The tempered dual phase steel may be lightly cold rolled for better surface finish and dimensional tolerance. The important parameters that control the microstructure of the dual phase steel produced in this manner are (i) chemical composition, (ii) microstructure of cast steel billet, (iii) hot-rolling temperature, (iv) nature and extent of manganese segregation, (v) amount of cold rolling, (vi) inter-critical annealing temperature, (vii) quench rate to transform austenite to martensite after inter-

critical annealing, and (viii) tempering temperature. Therefore, the processing-microstructure relationships are multivariate and complex.

2.1.3 Microstructure of Dual Phase Steels

Microstructure of dual phase steel contains two major constituents, ferrite and tempered martensite. In addition, very finely dispersed carbides of the micro-alloying elements (V, Ti, and/or Mo) are present in the microstructure; these carbides are not situated on the grain boundaries or ferrite-martensite interfaces. The volume fractions of martensite and ferrite are governed by the steel chemistry and inter-critical annealing temperature. In the majority of dual phase steels where tempered martensite volume fraction is in the range of 20-30%, ferrite is topologically continuous and contains dispersed discrete regions of tempered martensite. On the other hand, in the dual phase steels (such as the steel in this research) containing high volume fraction of the tempered martensite, the tempered martensite is topologically continuous and contains dispersed regions of ferrite.

2.1.4 Processing-Microstructure-Properties Relationships in Dual Phase Steels

Much work on dual phase steels has been carried out since they were first developed in the 1970's. The dual phase steels have been investigated for their chemical composition, thermo-mechanical processing parameters, heat treatment cycles, and differences in the microstructure [20,22,23,24]. The deformation and fracture mechanisms in the dual phase steels are dictated by their microstructure and chemistry; the microstructure is in turn governed by the processing. Consequently, for commercial

exploitation of these steels, it is necessary to understand the microstructural transformations with respect to the alloying elements and processing as they govern the final dual phase microstructure. The volume fractions of the ferrite and the martensite, the total surface area of the ferrite-martensite interfaces, size, phase morphology and distributions of the microstructural constituents have profound influence on the behavior of the dual phase steels. The overall stress-strain curve of dual phase steels can be controlled and modified by adjusting the constitutive phases and the above mentioned properties, which also influence the failure of the steels significantly. In-situ SEM experiments have been carried out by many researchers [25-28] to depict and understand the fracture process and fracture micro-mechanisms. On a macroscopic level much effort has been concentrated to understand the deformation behavior of dual phase steels by numerical, analytical and experimental methods. A brief survey of the processing-microstructure-properties relationships reported in the literature is given below.

A. Effects of Microstructural Banding

During the inter-critical annealing, the austenite nucleates in the regions of pearlite or at the grain boundary cementite particles followed by the rapid growth of austenite until the carbide is dissolved. Upon quenching these austenitic regions transform into martensite. Caballero et. al [24] did extensive work on the evolution of microstructure during the manufacturing process of dual phase steels. They found that a higher coiling temperature results in a higher amount of pearlite colonies being formed. Also a lower cooling rate from the coiling temperature the microstructure mainly consists of ferrite and pearlite. The micrographs obtained for samples at a higher coiling

temperature of around 650°c and samples for a lower cooling rate of 6°c/sec showed greater amount of pearlite and corresponding a higher degree of banding as compared to samples with a coiling temperature of 500°c and a cooling rate of 60°c /sec. This clearly signifies that a lower coiling temperature and a faster cooling rate significantly reduces the amount of pearlite formed and prevents the formation of bands in hot rolled steel products.

The influence of banding morphology- thickness, continuity, geometry, etc and banding phase properties has been studied from the tensile tests of the dual phase steels specimens and analyzed by in-situ SEM carried out, which enabled the understanding of the step wise fracture process taking place. Tasan et al. [29] reported that for continuous banded morphologies in DP 600 (a dual phase steel having strength of 600 MPa), highest local strains are observed in the narrowest section of the band leading to eventual void formation in the band. Intergranular shear bands intersect the martensite bands at exactly these critical (narrow) points causing the first voids to nucleate while the rest of the band shows no deformation. Thus shear bands are generated in preferential paths within the microstructure [17,27,28]. For dual phase steels, narrow band sections show drastic deformation to compensate for the low deforming wider sections of the band. The strains in these critical deformed regions are higher than even the most severely deformed ferrite regions. Strain maps at different stages of deformation revealed the micro-events taking place in DP steels: initially formation of slip lines in the ferritic grains takes place then localized deformation at around 45° to the tensile axis and the evolution of strain distribution from homogenous to heterogeneous with increasing deformation. These steps are similar in both pearlitic banded or in the case of dual phase martensitic banded steel.

But in the case of pearlitic banded structure, the strain partitioning is of less importance than in dual phase microstructures as pearlite can take the ferrite deformation as well [29]. Thus, for continuous microstructural bands, shear bands are produced and are forced to pass through the narrow sections of the band, and in this way, the banded martensitic phases is forced to deform beyond its plastic limit more so cause of the significant strain difference between the martensite and the ferrite. For discontinuous bands, the shear bands can circumvent this situation by naturally crossing the gaps and hence delaying early damage initiation. Therefore, to optimize the properties of a banded microstructure, it is imperative to avoid continuous bands in the final microstructure and also decrease the thickness variation so that some ends of the band do not bare more strain and eventually deform beyond the plastic limit.

B. Effect of Martensite and Ferrite Phases

Volume fractions of martensite and ferrite constituents and their microstructural geometry are dictated by the steel chemistry, inter-critical annealing temperature and numerous other process parameters [30,31]. Along with the microstructural volume fractions, the morphology of martensitic bands, their distribution in the microstructure, and the spacing of the bands play significant role in the damage evolution and fracture processes. He et al. [32] reported that in the steel having coarse band structures containing 17% martensite, the initial void formation occurs due to the cracking of the martensite at very low strain levels. Kim and Thomas [33] also reported that cleavage fracture occurs at ferrite in a coarse martensite structure, whereas in a fine microstructure, voids nucleate via decohesion at the ferrite-martensite interface. Figure 4 shows the

center part of DP600A steel microstructure with a non-uniform spatial distribution of martensite bands in the ferrite matrix- the microstructure shows martensite banding in the mid-thickness of the sheet and parallel to the rolling plane. Figure 5 shows DP600B steel microstructure with uniform martensite band throughout the steel thickness.

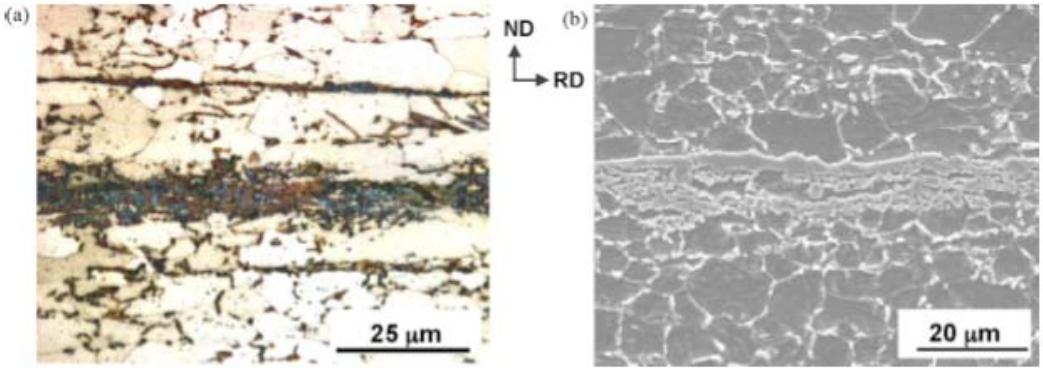

Figure 4: a) Optical micrograph of etched DP600 steel showing centerline martensite banding; b) Scanning electron micrograph showing the same. [27]

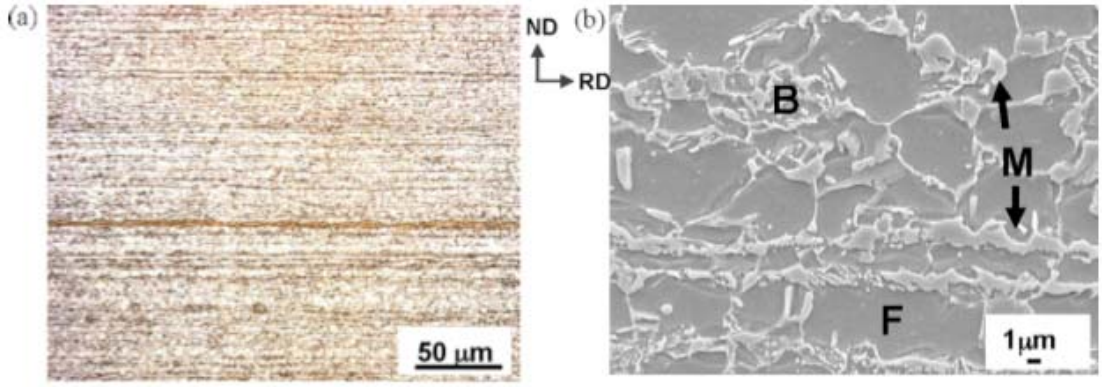

Figure 5: a) Optical micrograph of etched DP600 steel showing uniform martensite banding; b) Scanning electron micrograph showing the same. [27]

Figure 6 shows voids revealed by light microscopy in the thickness direction for the two grades of steels. It can be seen that the biggest voids in the DP600A is at the central – martensitic line region with sparsely distributes voids as we move away from the centerline. For DP600B there are strings of voids which are more uniformly distributed through the thickness. The void density increases towards the fracture.

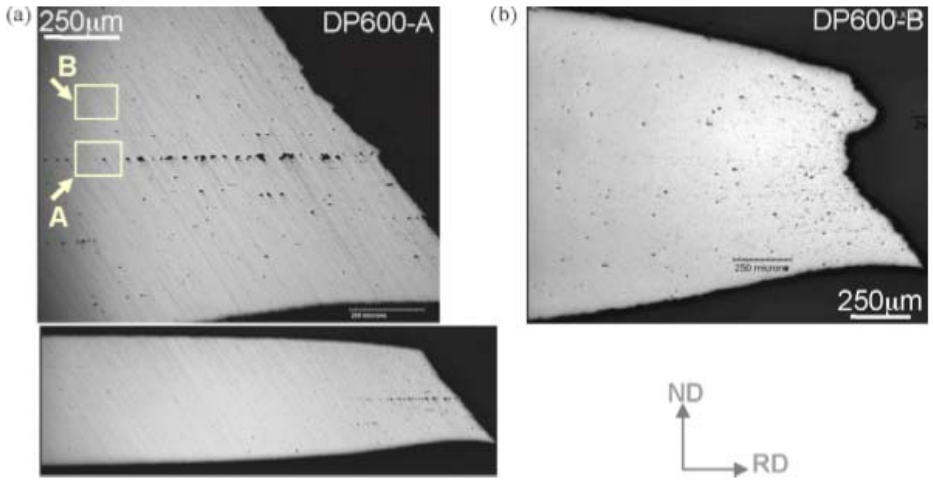

Figure 6: Voids in polished longitudinal sections a) DP600A steel; b) DP600B [27]

For steel DP600A three types of void nucleation take place- cracking of the martensite, separation of adjacent martensitic regions and decohesion at ferrite-martensite interface at regions away from the centerline. Thus in DP600A martensite cracking starts at low local strains. As deformation proceeds, the voids initiated at the martensitic bands grow further by an increase in the separation of the cracked martensitic regions rather by void nucleation resulting in the increase in the area fraction of the biggest void. At larger strains voids open between adjacent martensite particles and at the ferrite-martensite interface where finally the incompatibility of the stress distribution between the soft ferrite and the hard martensite dominates. At higher strains ferrite-martensite decohesion

takes place and voids grow into the ferrite and propagate in the direction of straining. In general dual phase steels with non-uniform distribution of martensitic bands show larger and deeper dimples towards the band [27,28]. On the other hand dual phase steels with uniform martensitic bands throughout the thickness of the specimen show that void nucleation occurs continuously throughout the deformation process. Primary mechanism for void formation is decohesion of the ferrite-martensite interface. Voids so formed grow along the ferrite grain boundaries without coalescing parallel to the direction of the applied load. Thus the ferrite phase can continue to deform without fracture. Voids that form in the neck region (tri-axial state) tend to coalesce transversely and eventually lead to the fracture of the steel. In summary, it is found that the microstructure with non-uniform martensitic bands in it, shows an accelerated damage with the overall damage evolution mainly due to the growth of voids previously nucleated at the martensite center line in the microstructure. In a uniformly distributed banded microstructure, void nucleation takes place continuously throughtout the fracture process. The fracture surface shows a uniform background of smaller dimples since there is only a small portion of the voids are created by martensitic cracking (at low strains) and so the ferrite continues to deform without fracture unlike the previous DP600-A where the martensite is the first to deform.

Shen et al. [28] studied the microscopic process of straining of the two phases in plain carbon dual phase steels. The martensite/ferrite strain ratio ‘R’ defines the degree of uniformity of straining between the two phases. As mentioned previously, in the case of dual phase steels with a ferrite-martensite microstructure, the strain partitioning plays an important role in dictating the fracture behavior. The study involved the effects of

microstructural parameters like volume fraction of martensite, its carbon content and tempering cycles on the strain behavior of dual phase steels. The initial stages of deformation were same as that reported by Tasan et al.[29] with the slip lines being localized in the ferrite grains as the steel begins to yield, these then propagating at angle of 45 (to the tensile axis) towards the martensitic islands as the macroscopic strain increases. Volume fraction of martensite V_M affects the strain distribution. Lower the value of the V_M and higher the value of $\%C_M$ lesser is the degree of deformation of martensite islands. With increasing V_M, the ferrite grains are increasingly constrained by the large martensite volume around it and therefore its contribution to the overall macroscopic strain is reduced. The microscopic strain of the two phases Σ_M and Σ_f increases linearly with the macroscopic strain of the specimen with the deformation of the ferrite phase occurring immediately, followed by the delayed deformation of the martensitic phase. Keeping the $\%C_M$ to be same, an increase in the V_M results in narrowing down the strain difference between the martensite and the ferrite phase. This basically signifies that if $\Sigma_{M'}$ is the value of the macroscopic martensite strain and Σn is the necking strain of the specimen, with a higher volume fraction of martensite, the martensite begins to deform soon after necking ($\Sigma_{M'}/\Sigma n = 1.05$) or in some cases even before necking occurs ($\Sigma_{M'}/\Sigma n = 0.82$). On the other hand if V_M is kept constant, then the degree of uniformity on strain denoted by the ratio 'R' increases with a decrease in the $\%C_M$ or in other words the microhardness of the martensite phase. This is also seen with an increase in the tempering temperature as both the cases result make the martensite phases deform easily due to its reduced strength. The increase in the $\%C_M$ makes the martensite deform much later after necking making the $\Sigma_{M'}/\Sigma n$ ratio close to 1.2 and a

decrease in the value $\%C_M$ results in a earlier deformation of martensite with $\Sigma_{M'}/\Sigma n$ = 0.84 as reported by Shen et al. in their study of DP steel samples. Thus the straining of the two phases and the starting point of martensitic deformation in DP steels is not uniform and depends on the microstructural parameters with V_M, $\%C_M$ having a profound influence on the $\Sigma_{M'}/\Sigma n$ ratio and the Σ_M/Σ_F ratio R.

Recent work by Colla et al. [34] characterizes the strain hardening behavior of conventional DP 450 and DP 600 steels. The tested DP steels were characterized by different alloying elements-Al, B and P and the mechanical properties so induced were found out and compared. The DP600P and the DP450P steels exhibit the highest values of the tensile and the yield strengths because of solid solution strengthening by P. These steels also do not exhibit the characteristic continuous yielding behavior of DP steels. The Al containing DP steels show the lowest content of hard phases. Al reduces the amount of austenite formed in the inter-critical annealing stage. With less austenite being formed more C is concentrated in the austenite thereby increasing the hardenability. Therefore as compared to DP450P and DP450B no bainite is formed in the final DP microstructure. The strain hardening behavior has been studied using constitutive equations of Holloman analysis, the Crussard-Jaoul (CJ) analysis and the modified CJ analysis, all of which are based on the Holloman, the Ludwik, and the swift equations [9,18,34].

2.1.5 Failure mode studies of dual phase steels

Numerous contributions report research on analytical and numerical modeling of the mechanical properties of dual phase steels. The mechanical properties of ferrite and martensite are different from each other, and taking this into consideration, Choi et al.

[8,9,35] have predicted the ductile failure of steels in the form of plastic strain localization resulting from the incompatibility in deformation between the two phases. Micromechanics-based finite element method is used in predicting macroscopic stress versus strain behaviors along with failure modes in DP 980 and DP 780 (lower volume fraction of martensite) steels under different loading conditions. The exercise demonstrates that microstructural inhomogeneity can be a key factor in influencing the ductile fracture of dual phase steels. The plastic flow stresses for the ferrite and the martensite phases are described by the following equations

$$\sigma_0 = \sigma_{y,F} + K_F \bar{\varepsilon}_{ep}^{n_F}$$

$$\sigma_0 = \sigma_{y,M} + K_M \bar{\varepsilon}_{ep} \qquad (1)$$

Here $\sigma_{y,F}$ and $\sigma_{y,M}$ represent the initial yield strengths and K_F and K_M represent the hardening coefficients for ferrite and martensite phases, respectively. The exponent n_F is the hardening exponent for the ferrite phase, while for martensite a linear hardening behavior is assumed. The finite element analysis in the study involved assumptions related to the ferrite-martensite isotropic hardening behavior under loading and also no prescribed failure criterion is used, with ductile failure being predicted as the natural outcome of plastic strain localization due to the incompatibility in deformation between the two phases. *Decohesion of ferrite martensite interfaces leading to interface fracture is completely ignored in these computations. Further, the finite-elements (FE) based computations are performed on two-dimensional (2D) microstructure images although the real microstructures are three-dimensional (3D). In addition, the FE based computations are performed on small windows of the SEM microstructural images, which may not necessarily be truly representative (and hence RVEs) of the global*

microstructure. Therefore, these numerical modeling results are unrealistic, particularly because experimental observations clearly reveal that fracture along ferrite-martensite interfaces is an important fracture mode. The FE based computations predict that the UTS increases with an increase in the initial yield strength and the martensite hardening rate but the UTS strains and the failure strains are found to decrease with an increase in the initial yield strength and the hardening rate. As a consequence of the martensite mechanical properties mentioned above on the stress-strain plots, it is suggested to have lower martensite initial yield strength and hardening rate. With these conditions, failure of the RVE as suggested by the finite element analysis is by pure shear and shear-dominant failure modes.

A decrease in the volume fraction of martensite leads to a decrease in the ability of the martensite to deform [8,21,25,28]. Therefore the initial yield strength of martensite has little influence on the UTS and the UTS strain as noticed in the RVE in the case of DP 780 steel with a lower volume fraction of martensite than DP 980. The failure strain is considerably larger for lower initial yield strength and hardening rate of martensite. The extensive study in the end revealed that lowering the initial yield strength, hardening rate and volume fraction of martensite results in a decrease in the strength of the steels (UTS) but the UTS strain and the failure strain increases. Thus martensite mechanical property has striking influence on the failure mode of dual phase steels and can be used as a design criteria for developing new grades of dual phase steels.

The damage characteristics of the dual phase steels have been extensively studied using in-situ SEM experiments [25-28,36] and using X-ray microtomography. G-Avramovic-Cingara et al.[25] have described void nucleation and growth using

quantitative data. The rate of void nucleation is dependent on many parameters like martensite volume fraction, the size and distribution, its morphology all of which have been discussed in this chapter previously. The study on DP 600 steels revealed that void nucleation occurs generally on the interface perpendicular to the tensile axis and these voids then grow along the ferrite boundaries. Voids that are formed under traiaxial state of stress as those in the neck region grow and coalesce in the thickness direction of the tensile specimen leading to ultimate separation and failure. A small percentage of the voids are also formed by the fracturing of the martensite on the interface perpendicular to the tensile axis but they do not seem to grow significantly. Quantitative measurements on the damage evolution revealed that the void area fraction increased with an increase in the thickness strain while approaching the fracture surface. However the average void area and the average void size decrease with strain. This is due to continuous void nucleation mechanism occurring in dual phase steels. E.Maire et al.[36] developed a model to describe the damage initiation and evolution in dual phase steels. The qualitative results in the study were obtained by X-ray tomography which showed the 3D rendering of outer surface of the cavities formed, first for the initial state and then for the state just before fracture. It revealed that the fraction of the pores remained constant when the tensile stress was homogenous but a substantial increase was observed when triaxial stresses set in during necking. The density of cavities is heterogeneous and is maximum at the center which corresponds to the higher stress triaxiality induced due to necking. Here the outer shape of the sample is used to determine the value of the local tensile stress at the center. This assumption is not so accurate in cases where necking is pronounced. This is also used to calculate the value of the stress triaxiality at the center T

$= \sigma_m/\sigma_{eq}$ where the numerator and denominator represent the hydrostatic part and Von Misses equivalent part of the stress tensor respectively. Here the Bridgeman approximation is used to calculate it which assumes that the sample is axissymmetric. This assumption may not be accurate in the case of dual phase steel tensile specimens. Nevertheless the exercise clearly shows the quasi-stagnation of the average equivalent diameter which occurs due to the competition of the growth of the existing voids to the nucleation of new ones. A model was hence developed to predict this stagnation of cavities for dual phase steels. The model was based on the classical Rice and Tracey approach which combines progressive initiation with growth.

$$\frac{dR}{R} = 0.238 exp\left(\frac{3}{2}\frac{\sigma_m}{\sigma_{eq}}\right) d\varepsilon.$$

The model used describes the growth of the radius R of the cavity assuming the matrix is perfectly plastic. A linear relationship between the growth rate and an increase in the plastic strain is observed.

Thus though considerable amount of work on fracture behavior of dual phase steels has been carried out through developments of analytical and numerical method analysis, the quantitative data obtained through models are based on a large number of *unrealistic* assumptions. None of the models and simulations reported in the literature can predict the variability in the ductility in a set of specimens where all *average global microstrucutral parameters (volume fractions of the phases, total surface area of the interfaces, etc.)* are the same. Therefore, a new generation of models and numerical computation algorithms that account for experimental fractographic data and observations need to be developed. The first step in such a process is systematic experimental fractographic work that can relate the observed variability in the ductility to

the measured fractographic parameters. Accordingly, the present work on dual phase steels intends to quantify the fracture surfaces of dual phase steels based on experimental observations using SEM and profilometry-based techniques. To the authors best knowledge such quantitative data on fractography and in-turn delineating the prominent failure mechanisms in dual phase steels hasn't been reported before, and therefore, the results shown in the subsequent chapters provide new insights into microstrucutral origins of the observed variability in tensile ductility in the dual phase steel of interest.

The above literature review of processing-microstructure-properties relationships in dual phase steels reveals that there have been numerous in-depth studies reported in the literature on the relationships between *average* microstructural parameters and the *average* mechanical properties of the dual phase steels. Nonetheless, none of the studies reported in the literature concern the *variability* in the fracture sensitive properties of the dual phase steels and its relationships with the microstructural variability. The present research involves extensive quantitative microstructural and fractographic measurements to understand the microstructural origins of the variability in the tensile ductility (which is a fracture sensitive property) of a dual phase steel. The stereology and digital image analysis techniques, and the quantitative fractographic techniques utilized in the present work are reviewed in the next two sections.

2.2 Stereological Techniques

In general, all microstructures contain volumes of the constituents dispersed in the three-dimensional (3D) microstructural space; grain boundaries and interfaces among the microstructural phases/constituents; one-dimensional features such as dislocations and grain edges; and zero-dimensional points such as grain corners (quadruple points). Therefore, microstructures can be quantitatively characterized and mathematically represented via estimation of important geometric attributes of these basic geometric features. It is important to recognize that microstructures are three-dimensional (3D), and they are of stochastic nature. Consequently, geometric attributes of 3D microstructures are related to their mechanical and physical properties. Therefore, characterization of 3D microstructures is of core interest. Nonetheless, it is convenient to observe microstructures in two-dimensional (2D) metallographic sections or projections (as in TEM). As a result, unbiased, assumption-free, and general statistical relationships are needed to estimate the geometric attributes of 3D microstructures from the measurements performed in the 2D metallographic sections or microstructural projections. Such relationships are provided by stereology [12]. A brief overview of the stereological relationships used in the present research is given below.

2.2.1 Estimation of Volume Fraction

Volume fraction is a quantitative measure of the relative amount of a given phase in a mixed microstructure. It is one of the most important and the most frequently characterized microstructural attribute. The volume fraction of any phase in a three dimensional microstructure can be found out by calculations on two dimensional

micrographs obtained by standard optical microscopy without involving any assumptions concerning sizes, shapes, orientations and locations of the microstructural features. The volume fraction can be estimated by areal analysis, lineal analysis, or by point counting.

In 1848, French geologist Delesse [11,12] developed the areal analysis technique for estimation of volume fraction. The areal analysis involves measurement of the fraction of the area of metallographic plane occupied by the phase of interest or constituent. It is denoted by A_A. Image analysers can be used to give the absolute area of the tracing or the feature of interest. The average value of the area fraction of a given phase on a 2D metallographic plane is an unbiased estimator of the volume fraction of that phase in 3D.

The lineal analysis involves using test lines as opposed to the use of test planes in areal analysis. Here, the fraction of the test line passing through the given phase is measured and an average value of this length fraction L_L gives the volume fraction of the phase of interest in the 3D microstructure. The relationship is completely general and is applicable to any arbitrary microstructure. The point fraction technique which is less tedious than the previous two methods involves placing a grid of points on the 2D metallographic plane and calculating the fraction of the grid points that fall on the phase of interest. The average value of this fraction of grid points P_P is an unbiased estimator of the volume fraction in 3D. It has been proved that systematic random sampling is more accurate than random sampling as it leads to uniform sampling of the microstructure and efficiently averages over region-to-region variations in the microstructure.

The stereological relationships for volume fraction estimation can be summed up as :

$$V_V = A_A = L_L = P_P \qquad (2)$$

2.2.2 Estimation of Surface area per unit volume

Microstructures often contain internal surfaces or boundaries such as grain boundaries, precipitate-matrix interfaces, inter-phase boundaries etc. These microstructural features strongly affect the mechanical and physical properties of materials. The intersection of internal surfaces distributed in a three dimensional reference volume with a metallographic plane gives lines or traces that can be seen using standard metallographic techniques. Though significant information regarding the geometric attributes is lost when the dimensionality is reduced by one to 2D in metallographic planes, the total surface area per unit volume can be estimated in an unbiased fashion using stereological techniques on 2D metallographic planes. The total surface area per unit volume is denoted by Sv and is defined as the sum of the total surface areas of all the internal surfaces of interest contained in a reference volume divided by the same reference space Vo. Sv is not a dimensionless quantity like Vv and therefore magnification of the microscope is important to obtain an accurate estimate of the total surface area per unit volume. The method for determination involves sampling the microstructure so obtained by using test lines and counting the number of intersections made by the test lines with the phase of interest. The average number of intersections normalized by the test line length gives the count of the intersection per unit test line length denoted by P_L . These calculations are repeated at different locations in the microstructure and an average value of the number of these intersections per unit test line length is calculated [11,12]. The surface area per unit volume Sv is related to this intersection per unit test line length P_L by the general equation

$$Sv = 2 \langle P_L \rangle \qquad (3)$$

This equation is applicable to microstructures of any shape, size and orientation etc.. For a microstructure having randomly oriented features, any orientation of the test line is random with respect to the microstructure. So calculation on a single metallographic plane is enough to give an unbiased estimate of Sv. If the microstructure is anisotropic, it is essential to perform the measurements with test lines of different orientations and planes of different orientations in three dimensional space. Baddely et al. [35] showed that a set of planes having one common axis, which is called the 'vertical axis' contains test lines of all possible angular orientations in 3D. The set of planes that contain the vertical axis are called the vertical planes. Since any set of vertical planes contain lines of all possible orientations, it is possible to get an unbiased estimate of Sv by calculations on one of the vertical planes. However the line intersection count made by straight lines needs to weighted by the average of the sine of the angle between the test line and the vertical axis to give equal weight to all test lines of all orientations. For this purpose cycloid shaped test lines are used instead of straight lines. The cycloid shaped test lines are so drawn so that their minor axis is parallel to the vertical axis. The equation for Sv then changes to a general equation

$$Sv = 2 \langle P_L^{cyc} \rangle \qquad (4)$$

Gokhale and Drury [37] have proposed an efficient technique to calculate an unbiased estimate of Sv in anisotropic microstructures where a symmetry axis is absent. The method involves sampling of the microstructures by using three metallographic planes containing the vertical axis at angle of 120° with each other and containing lines of different orientations. This procedure is most efficient when the vertical axis so chosen is not parallel to most of the surface elements of interest.

2.2.3 Estimation of Two-Point Correlation function

Correlation functions are useful to describe the geometry of a microstructure. These are statistical descriptors that implicitly contain information about the metric and the topological properties, the spatial (clustering etc.) and morphological anisotropy of microstructures. The volume fraction measurements give the relative amounts of the respective phases but the influence of the spatial distribution of the phases in this case banding in the microstructure can be understood by using the two point correlation functions. They are extensively used to match the experimentally measured descriptors with that of simulated microstructures to make sure they match well with the real microstructures. N-point correlation function P ($r_1.r_2,r_3$…..) is the probability that a polyhedron of given size and shape with n vertices when placed on a microstructure has all the n vertices lying on the particles or a given phase of interest. If the microstructure contains two phases with phase 1 being any particle, inclusion and phase 2 being the matrix then n-point correlation function can be defined for phase 1 if all the n points fall on phase 1 and similarly n-point correlation for phase 2 when all the vertices lie on phase 2, the matrix. Depending on the number of vertices and the geometry of the polyhedron different number correlation functions can be defined. The smallest order correlation function is the 1-point correlation function which involves a random point being placed in a 3D microstructure and the probability of the point falling in a given phase. The two-point correlation, which is usually used for statistically homogenous media can be obtained by tossing a line segment of various lengths $r = |r|$ with a specified orientation into the microstructure and counting the fraction of times the ends of the line segment fall in a given phase of interest. The probability function can be defined as $P_{ij}(r,\theta,\phi)$ where i

and j can be 1 or 2. P_{11} with both the end points falling in phase 1, P_{22} with both the end points falling on phase 2 the matrix and P_{12} or P_{21} with the end points one in phase 1 other in phase 2. Figure 7 below illustrates the two-point correlation.

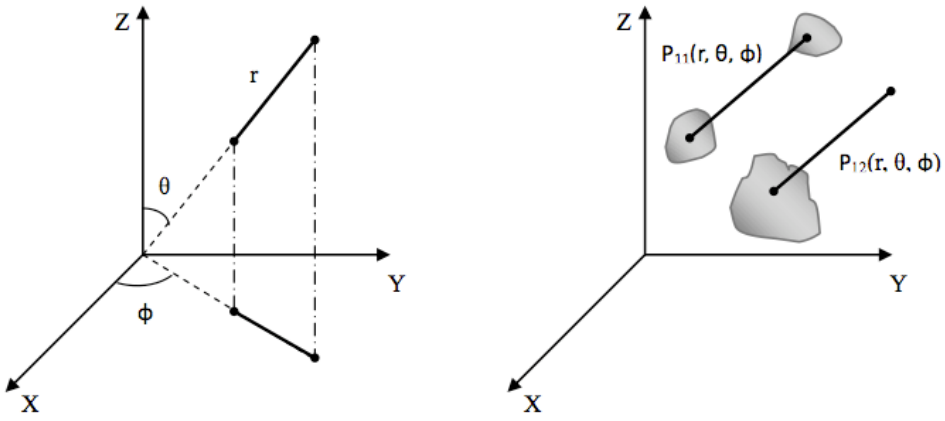

Figure 7: Schematic of a two-point correlation function.[40]

The point to be noted here is that the probability function is concerned only with the end points of the line segment and the events associated with it. For a two phase microstructure as in the case of dual phase steels there are four possible two-point correlation functions as mentioned previously. However only one of the four two point correlation functions is independent as the following equations exist [39,40].

$$P_{11}(r,\theta,\phi) + P_{22}(r,\theta,\phi) + P_{12}(r,\theta,\phi) + P_{21}(r,\theta,\phi) = 1 \quad (5)$$

$$P_{12}(r,\theta,\phi) = P_{21}(r,\theta,\phi)$$

$P_{11}(r,\theta,\phi) + P_{12}(r,\theta,\phi) = f_1$ where f_1 is the volume fraction of phase 1

The following well known limits exist for the values of two point correlation functions as r approaches zero and r approaches infinity. The limits being completely general make these equations valid for random as well as non-random microstructures.

$$\lim P_{ij}(r,\theta,\phi) = f_i \qquad \text{when } i=j \text{ and } r \to 0 \tag{6}$$

$$\lim P_{ii}(r,\theta,\phi) = [f_i]^2 \qquad \text{when } r \to \infty$$

$$\lim P_{ij}(r,\theta,\phi) = [f_i]\,[f_j] \qquad \text{when } r \to \infty$$

At other values of the length of the line segment r, the two-point correlation function depends on the first order global properties of the microstructures as well as on the spatial arrangement of the features and their anisotropy. In the present work the two-point correlation function is sought out to distinguish the effect of banding in various dual phase steel specimens as it contains information about the first order properties including the morphological anisotropy, which in the present work is considered as a source of variability.

2.3 Digital Image Analysis

Digital image analysis involves extracting useful information from microstructures via estimation of the geometrical attributes of the features in a metallographic plane. Three dimensional microstructures are characterized by observations and calculation using stereological techniques on these two dimensional metallographic planes/micrographs. The image analysis system that is generally used in a metallography lab consists of a computer which automatically studies an image and

extracts important qualitative and quantitative information out of it, a software like KS400 or Axio which can process the image and carry out measurements on it and an interface which transfers the image captured by the microscope to the computer screen. This is the CCD camera. The usual paraphernalia associated with this whole setup may comprise of an automated stage or a focusing mechanism all to enhance the image quality and subsequently make the quantitative measurements more efficient.

A digital image is made up of pixels or dots. In an unprocessed black and white image the pixels can take up values from 0 to 255. 0 being completely black and 255 being completely white. These levels are known as gray levels. A colored image on the other hand has three main color components red, green and blue. All possible color combinations are possible using these three basic colors each having its own set of gray scale values from 0 to 255. When an image is captured by a microscope, it gets stored in the form of a pixel map with the positions of the pixels giving the various color combinations and gray scale levels. The gray scale image has to be converted into a binary image before any calculations can be done on it by the image software. A binary image consists of only white and black pixel levels with no range of gray scale values. The process of converting a gray scale image to a binary image is knows as 'thresholding' or in common image software terms 'segmentation'. In this process all pixel value below a certain fixed gray scale value is taken as 0 or black and all other pixel values above it as white. Once this is done, the image has to be identified i.e. all separate features have to be tagged and only then the image is available for measurements to be performed on it. The measurements performed on these binary images are carried out in the units of pixels i.e. the measured area is reported as the total number of pixels enclosed

by the feature of interest. These pixel calculations have to be converted to micron for which the calibration table of the microscope in use is needed or a calibration slide in general to get the conversion factors. The calibrations should be performed in both the horizontal and the vertical direction, as the CCD has different magnifications in different directions. Once this done the data is stored in a file, which can be exported to spreadsheets, software to calculate statistical data such as average values, variance, standard deviation etc.

2.3.1 Montage creation

In many cases in a two phase microstructure, the volume fraction of the second phase is very low and hence they are sparsely distributed. In order to observe and focus on them accurately a higher magnification has to be chosen which has a trade-off as at high magnification the field of view is reduced which may not be desirable as the nearest neighbor particle of the second phase may not be in the same field of view but in an adjacent one. In order to obtain statistically reliable measures of microstructural parameters that are free of bias due to edge effects it is essential to carry out the calculation on large area of metallographic planes. In such a case it is desirable to take micrographs of adjacent fields and paste them together making sure they match each other perfectly. However this method is not as accurate as there is a limit upto which the micrographs can be pasted together. A new method has been developed at Georgia Institute of Technology. In this work by Louis and Gokhale [41] large area high-resolution microstructural montages are created. The first step involves grabbing a first field of view (FOV) which is arbitrarily chosen in the region of interest in the

metallographic plane. This image gets stored in the memory of the computer as an image file. The right border of about 60 pixel width of this image is recalled on the left edge of a blank image. This semi blank image is then displayed along with the live image. This results in a superimposed image on the left border (of the previous right border and live image) with the rest of the screen having live image. Using image software techniques, it is now possible to achieve superimposition of adjacent images to the highest accuracy, which circumvents the problem of the physical movement of the stage having a large least count. Thus by image acquisition and then stitching them together automatically a "montage" of contiguous fields is created in the computer memory without any loss of resolution. These fields are then treated individually and the distance related parameters are modified according to the position of the whole montage. This clearly takes care of the trade off mentioned earlier between high magnification and loss of resolution. The figure below depicts a montage of 20 fields of view.

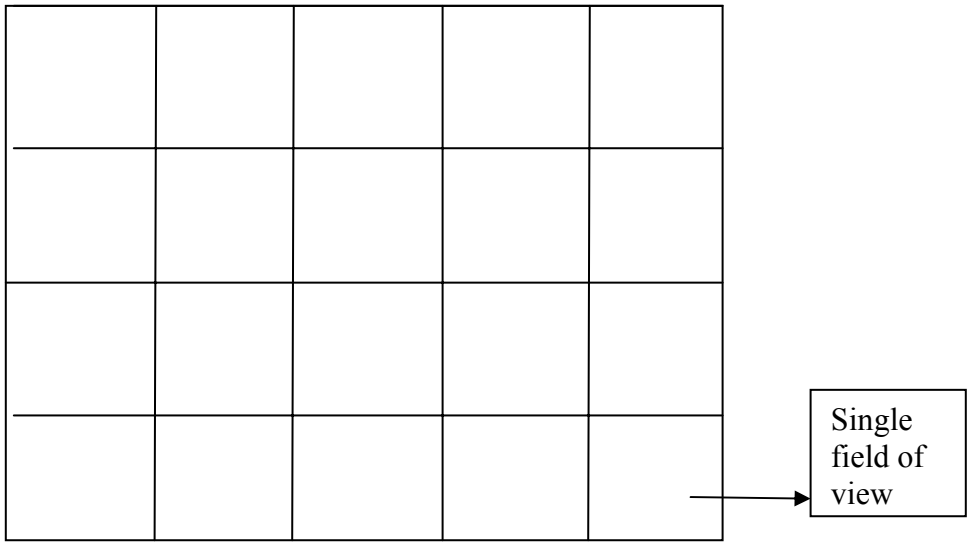

Figure 8: Schematic showing stitching of 20 fields of view to create a montage.

2.4 Quantitative Fractography

Fractography involves the study of fracture surfaces and is an important tool for understanding material fracture behavior. The deformation, damage evolution, and fracture process lead to generation of macroscopic fracture surface, which encodes great details about the microstructural features and fracture micro-mechanisms responsible for the global fracture. Therefore, microstructural features, loading conditions and the failure mechanisms usually determine the geometry and the topography of a fracture surface. A fracture surface, in general, is generated by the deformation and fracture processes operative at numerous length scales ranging from nanometers to millimeters. Therefore the study of the fracture surface geometry i.e. fractography, can provide useful information regarding the microstructural features and failure mechanisms that govern the material fracture.

Fracture can be qualitatively studied and described as ductile or brittle fracture (in some cases, a combination of the two) as indicated by the presence of features such as dimples, striations, beach marks, cleavage rivers, microvoid coalescence etc.. It gives the information on the roughness or smoothness of the surface, fineness or coarseness of the striations if present or whether the fracture was transgranular or intergranular. Quantitative fractography on the other hand gives a more objective description of the failure process. It is concerned with the quantitative characteristics of the geometric attributes of the fracture surface topography.

Modern quantitative fractographic techniques can be divided into – profilometry-based techniques, SEM-based techniques, three-dimensional fracture surface reconstruction methods and internal fractographic techniques. In all these techniques two

types of measurements are employed; individual or feature specific and field specific or global parameter measurements. The feature specific measurements involve information about geometry of specific features present on the fracture surface like number of dimples, striation spacing, average size of the inclusions on the fracture surface. Global parameters on the other hand are related to the global geometric attributes of fracture surfaces. The global properties can be estimated without any assumptions concerning the geometry of the specific features on the fracture surface. In the present research the SEM-based technique and the profilometry-based technique are used to find out both the feature specific and global parameters to characterize the tensile fracture surfaces of dual phase steels. The following section below provides a brief description of these parameters and the methods for their unbiased estimation.

2.4.1 Profilometry based quantitative fractography

A fracture profile is a tortuous line obtained by the intersection of a fracture surface with a 2D metallographic sectioning plane. Fracture profilometry plays an important role in estimating the global fracture parameters. It is of interest to quantify the global fracture surface topography in terms of few parameters which can be defined uniquely and can be estimated in an unbiased manner using practical measurements procedures. It is also important that these parameters are physically meaningful, so that they can be correlated to the dominant failure mechanisms, microstructure and material properties. Gokhale et al. [42,43] have proposed fracture surface analysis using an important global attribute of the global fracture- fracture roughness parameter (Rs). It is

defined as the ratio of the true area of fracture surface, S and its apparent projected area, A. Figure 9 illustrates this.

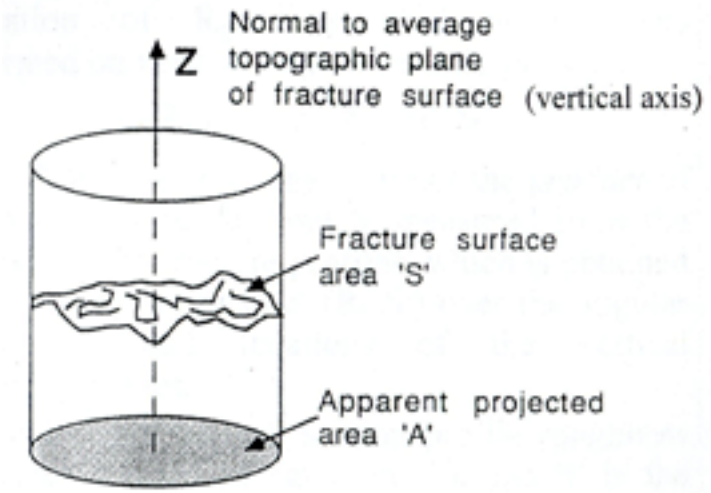

Figure 9: Schematic showing fracture roughness parameter.[42]

$$Rs = S/A \tag{7}$$

Rs can be estimated from the measurements performed on fracture profiles generated by intersections of fracture surface with metallographic planes. The fracture profile roughness parameter R_L is equal to the ratio of the true profile length L_t and the apparent profile length L'.

$$R_L = L_t / L' \tag{8}$$

R_L can be estimated from the vertical section planes as shown in figure.

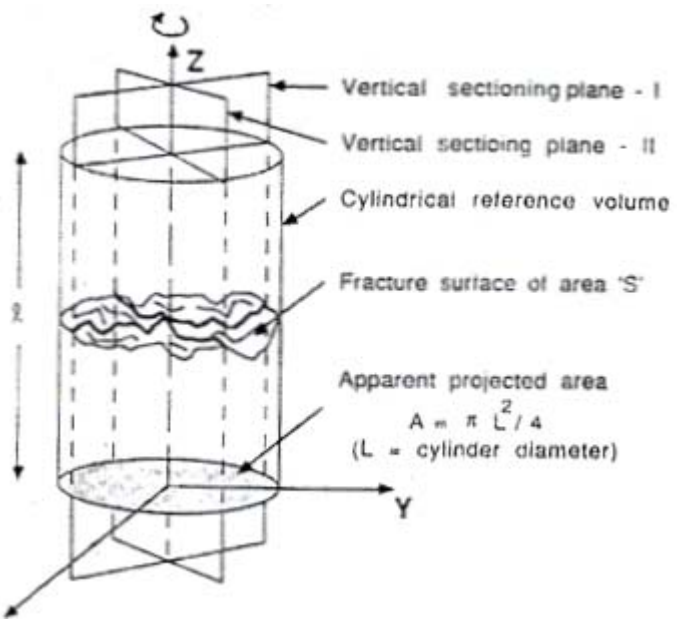

Figure 10: Schematic showing vertical section fracture profile.[42]

Experimental R_L values between 1.06-2.39 have been reported for various materials [42]. The surface roughness parameter Rs can be found out by the experimentally measured profile roughness parameter, R_L by using the following equation developed by Gokhale and Underwood [43].

$$Rs = \langle \Psi . R_L \rangle \tag{9}$$

where,
$$\Psi = \int_0^{\pi} [\sin\alpha + \{(\pi/2 - \alpha)\cos\alpha\}]\, f(\alpha).d\alpha \tag{10}$$

Ψ is called profile structure factor, and $f(\alpha)$ is the orientation function of the fracture profile and is defined such that $f(\alpha)d\alpha$ is the fraction of the profile length in the orientation range α to $(\alpha + d\alpha)$, where $0 < \alpha < \pi$. Here α is the angle between a line element in the vertical section fracture profile and the vertical axis. Detailed calculation of the profile structure factor involves numerical analysis; a computer code is available for this purpose.

2.4.2 SEM Fractography

SEM based fractography provides rapid examination of the fracture surfaces on a qualitative and quantitative scale using stereological techniques. In general cases it requires no special sample preparation. It is useful for quantitative characterization of specific features in terms of number density, average size, orientations etc.. It is particularly useful in estimating the area fractions on the fracture surface due to different failure mechanisms like dimple fracture, cleavage fracture or quassi-clevage fracture. All this can be obtained on a qualitative scale by seeing the fractographs, but giving an unbiased estimate of the dominant failure mechanism can be done using point counting as explained in the previous section for the estimation of volume fraction. The value obtained A_A through point counting on sufficient fields of view gives an unbiased estimate of the fraction of the fracture surface area generated by ductile failure mechanism by calculating the area fraction of the dimple regions, or by cleavage failure mechanism by calculating the area fraction of the cleavage regions.

$$P_{P(\text{feature of interest})} = A_{A(\text{dominant fracture mechanism})} \tag{11}$$

This has been carried out in the present research, details of which are explained in the next chapter. The quantity A_A so calculated is the area fraction of the SEM image so obtained. It is not equal to the area fraction of the fracture surface as in the SEM image only the projected area is visible. The true area fraction 'F' which represents the fraction of the fracture surface area in 3D is given by:

$$F = [Rs / (Rs)_\beta] \langle P_P \rangle = [Rs / (Rs)_\beta] A_A \tag{12}$$

Where Rs represents the fracture roughness parameter obtained through profilometry studies. Therefore Rs is required to correct SEM data for projections effects.

Number per unit area of SEM image, Ns can also be obtained. This is again obtained by the unbiased sampling of the field of views from the population of fields contained in the fracture surface. Unbiased counting of the features of interest is carried out using a frame of area smaller than the area of field of view on which it is superimposed. Consider figure 11:

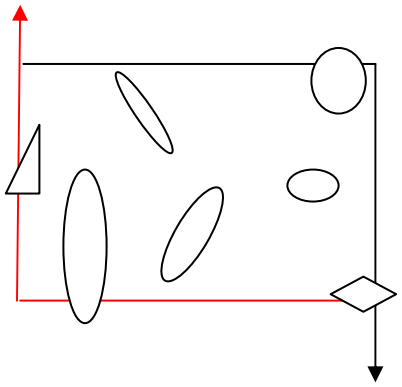

Figure 11: Shows an unbiased counting frame and the method of counting the number of features of interest.

In the figure the red edges are termed as 'forbidden edges' and any feature intersecting it is counted as zero. All other features which are completely inside the counting frame as well as those intersecting the black edges but not the red forbidden edges are counted as one. Therefore for the figure the number of features in the drawn rectangle is 4. In general the number of features per unit area of the SEM image Ns is given as [14]:

$$Ns = \langle N \rangle / \{A/M^2\} \qquad (13)$$

A is the area of the SEM frame and M being the magnification. Here also to correct for projection effects to represent the average number of feature per unit area of the true fracture surface represented by N_f , the fracture roughness parameter Rs is used.

For Ns the normalization carried out was with respect to the SEM frame area whereas for N_f it is the true fracture surface area.

$$N_f = Ns / Rs \tag{14}$$

Estimation of the *average size of the dimples* can also be obtained from the SEM fractographs. Here to take into consideration for the projection effects the value of F and N_f so calculated is used to give the true average size of the dimples on the true fracture surface area. The true average dimple size is given by Ω[13,14]:

$$\Omega = F/ N_f \tag{15}$$

CHAPTER III

EXPERIMENTAL WORK

3.1 Introduction

The prime focus of the current research is to understand the microstructural origins of variability in the uniaxial tensile ductility of a cold-rolled continuously annealed dual phase steel. For this purpose, experimental work has been carried out on tensile test specimens of a commercial cold-rolled continuously annealed dual phase steel. ArcelorMittal Global R&D, East Chicago provided the dual phase steel; carried out the thermo-mechanical processing; and performed the tensile tests. Quantitative microstructural and fractographic characterization of these specimens was performed at Georgia Tech. The microstructure characterization involved applications of stereology and digital image processing techniques as well as quantitative SEM fractography and fracture profilometry techniques described in the previous Chapter. The details of the material chemistry, processing, and the tensile tests are given in the next section of this chapter. The subsequent sections describe the metallography, microstructure characterization, and quantitative fractography of the specimens under investigation. The bulk three-dimensional microstructure as well the three-dimensional microstructure just below the fracture surfaces has been quantified, and fracture profilometry has been used to quantify the relationship between the fracture path and the microstructural constituents. These experimental data have been analyzed in the next Chapter to understand the relationships between the observed microstructures and the observed variability in the tensile ductility of the dual phase steel specimens.

3.2 Materials and Processing

3.2.1 Material Chemistry

The experiments were performed on commercial dual phase steel provided by ArcelorMittal Global R&D. The bulk chemical composition of the steel is given in Table 2.

Table 2

Chemical composition of the dual phase steel studied in wt%

% C	%Mn	%Si	%Mo	%Nb	%Ti	%Al	%P	%S
0.0934	2.15	0.6	0.1	0.012	0.015	0.042	0.0035	0.0014

Note that the carbon content of this steel is lower and the Mn content is substantially high in these dual phase steels to achieve martensite volume fraction higher than 50% in the processed steel (see section 2.1.1 of Chapter II for details). This steel chemistry also facilitates formation of dual phase microstructure where martensite is topologically continuous phase. The micro-alloying elements Ti, V, and Mo are added to retard the austenite grain growth during hot-rolling, and Si is added to decrease the tendency of cementite precipitation, which in turn facilitates martensite formation subsequent to inter-critical annealing.

3.2.2 Material Processing

The thermo-mechanical processing and heat treatment of the steel were performed at ArcelorMittal commercial flat products manufacturing facility. Cast steel slabs (typically, ~ 225 mm thickness) were hot-rolled at about 1200 °C to reduce the thickness

to about 4 mm. The hot rolled slabs are then cooled to room temperature. Hot-rolled steel has ferrite-pearlite microstructure. The hot-rolled steel was cold-rolled to further reduce the thickness (to about 2 mm). The schematic description of the inter-critical annealing treatment, subsequent quenching, and tempering treatment given to the present dual phase steel is given in Figure 13. After cold rolling, the incoming coil is subjected to continuous annealing process where it is heated to the inter-critical annealing temperature (AT). It is then slow cooled using gas jet cooling (GJC) followed by water quenching (WQ) at a rate of about 1000°/sec. The steel is then tempered at low temperature (OAT) to produce the final dual phase structure at room temperature.

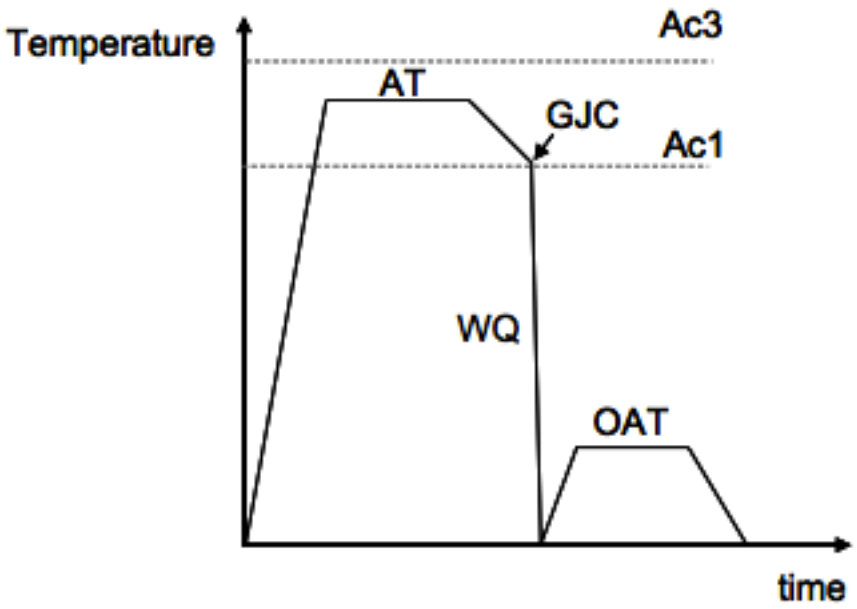

Figure 12: The heat treatment steps carried out to get the present dual phase microstructure.

3.2.3 Tensile Tests

The blanks for tensile test specimens were cut from different locations of two coils of the dual phase steel as illustrated in Figure 13. These tensile test specimen blanks were oriented parallel to the width direction of the coil. Tensile test specimens were machined from these blanks. The geometry and dimensions of the machined tensile test specimens are given in Figure 14 (JIS #5). The gauge section of the specimens is 63.5mm in length with the total length of the specimen being 230mm. The width of the gauge section is 24.9 +/- 0.25 mm. This specimen geometry facilitates generation of fracture in the central portion of the gauge length.

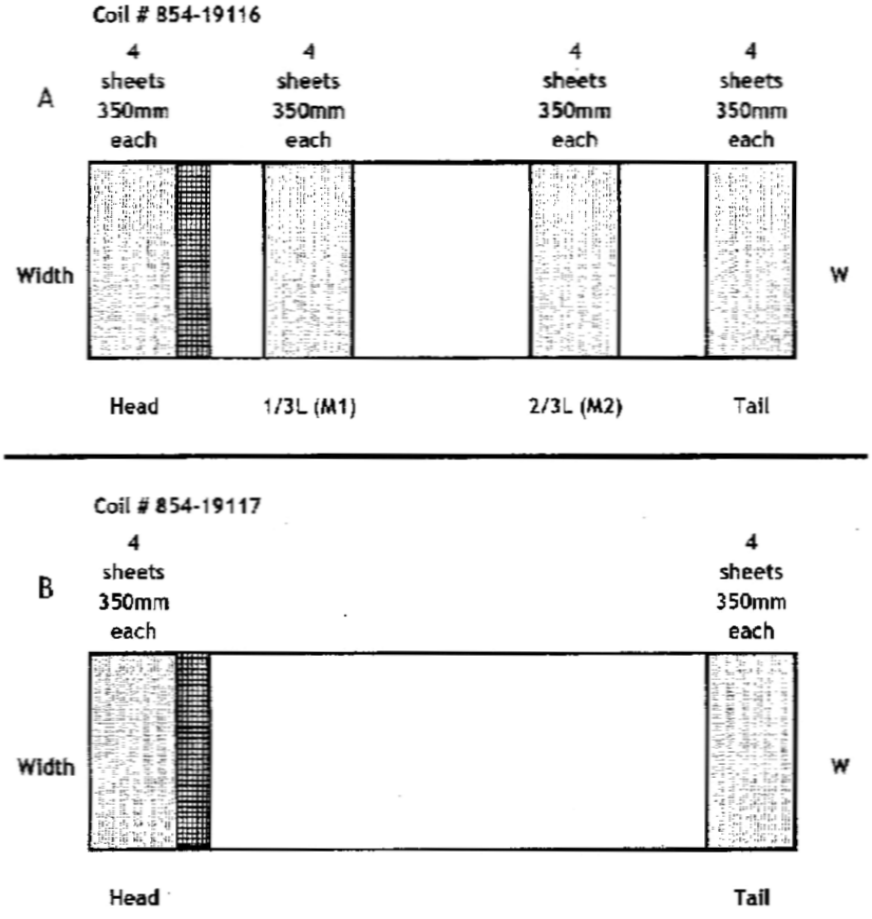

Figure 13: Schematic showing the location of the samples cut from the coils.

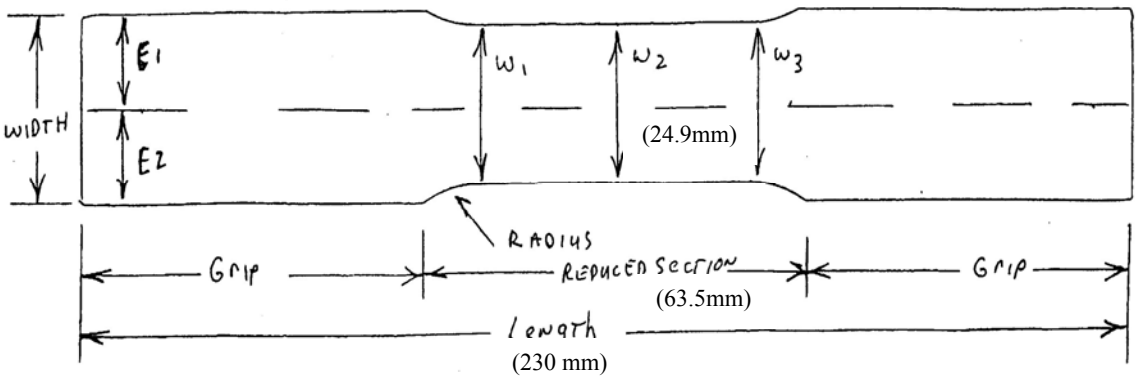

Figure 14: The tensile test specimen geometry.

The uniaxial tensile tests were performed at room temperature using screw driven InstronA testing machine. The tests were performed in a displacement-controlled mode. The tensile properties of interest that were recorded are yield stress, ultimate tensile stress, uniform elongation and total elongation. Table 3 a) below lists the tensile properties of the dual phase steel samples that were cut from two coils. The ductility (a fracture sensitive property) varies from 10.1% to 15.8% (a variation of more than 50%), although the yield stress (which is not a fracture sensitive property) varies at the most by 7%. Table 3 b) shows the samples selected from a) with varying total elongation that were used for characterization.

Table 3

a) Room temperature uniaxial tensile properties of the dual phase steel samples cut from two different coils having the same chemical composition and heat treatment.

COIL ID	POSITION	SPECIMEN NO.	E, GPa	YS, MPa	TS, MPa	TE, %	UE, %
854-19116	HEAD	1	230	679	1021	14.9	7.1
		2	235	698	1021	14.6	6.8
		3	234	673	1021	15.4	7.3
		4	239	672	1013	14.4	7.0
		5	221	697	1025	14.4	6.9
	1/3 L	1	222	696	1015	13.8	6.7
		2	233	676	1016	14.2	6.9
		3	226	691	1018	14.2	6.9
		4	224	695	1017	13.5	6.6
		5	238	688	1024	14.6	7.0
	2/3 L	1	246	666	1017	15.5	7.2
		2	163	695	1019	14.5	7.2
		3	226	699	1022	14.6	7.0
		4	249	678	1025	14.6	7.0
		5	248	678	1024	14.5	7.0
	TAIL	1	230	679	1022	15.0	7.0
		2	228	695	1014	13.6	6.5
		3	241	663	1017	14.0	6.6
		4	222	700	1025	11.9	6.4
		5	222	701	1021	10.1	6.1
854-19117	HEAD	1	233	660	1023	15.8	7.5
		2	232	669	1026	15.8	7.5
		3	244	661	1027	14.3	7.2
		4	263	666	1032	14.0	7.0
		5	242	667	1031	12.7	6.8
	TAIL	1	218	684	1060	14.4	7.0
		2	225	694	1052	13.9	6.7
		3	215	681	1046	14.7	7.1
		4	228	677	1052	13.1	6.4
		5	219	675	1044	15.6	7.1

Table 3

b) Room temperature uniaxial tensile properties of the dual phase steel samples used for characterization.

Specimen Number	Yield Stress (MPa)	Ultimate Tensile strength (MPa)	Uniform Elongation (%)	Total Elongation (%)
1	701	1021	6.1	10.1
2	700	1025	6.4	11.9
3	677	1052	6.4	13.1
4	663	1017	6.6	14.0
5	660	1023	7.5	15.8

Figure 15 shows the uniaxial tension test stress-strain curves for the two extremes-highest and the lowest ductility samples.

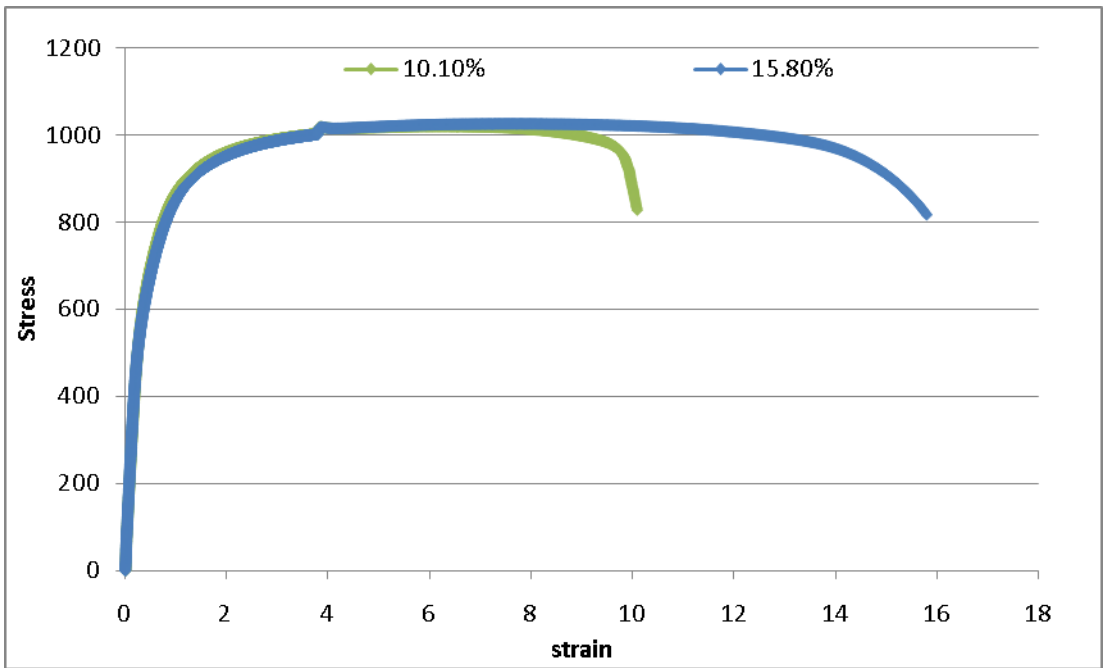

Figure 15: Eng. Stress Vs Eng. Strain for the two dual phase steel samples having the highest and the lowest total elongation values.

3.3 Metallography

An important part of microstructure characterization is metallographic specimen preparation technique that can clearly reveal relevant aspects of the microstructure such that a sufficient contrast is present to distinguish between tempered martensite and ferrite constituents in the dual phase microstructure. In the present work, representative global microstructure as well as the local microstructures just below the tensile fracture surfaces have been characterized. To characterize representative global microstructure, the specimens were sectioned along three orthogonal sectioning planes to reveal the

microstructures in longitudinal sections, planar sections, and transverse sections, whose orientations are given in Figure 16. For characterization of fracture profiles and local microstructures just below the fracture profiles the planar section regions just below the fracture profiles were utilized.

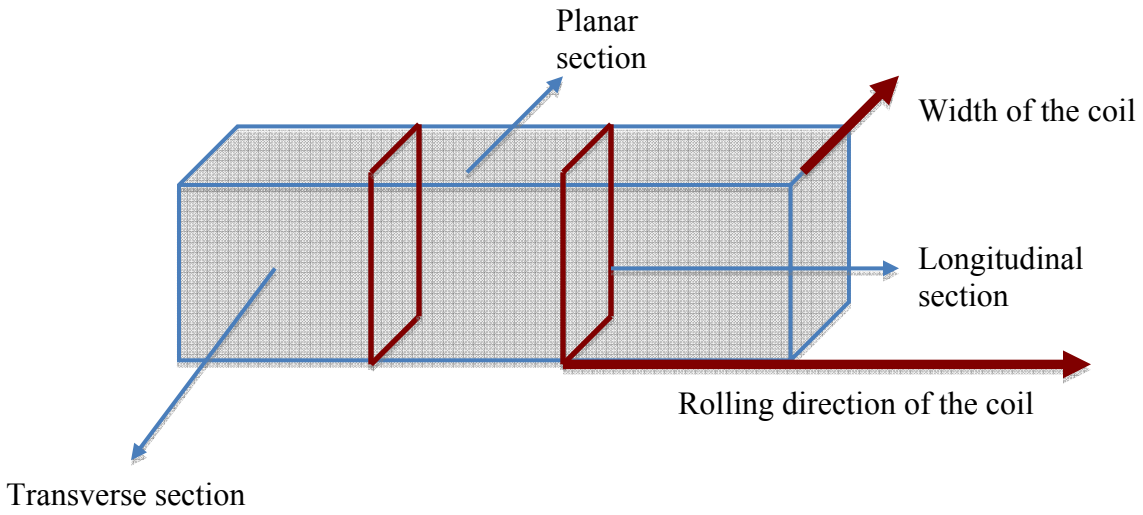

Figure 16: Orientations of microstructural sectioning planes.

The specimens were mounted using a cold mounting polyester resin and hardener along with ruby red dye. The dye was basically added to make the mount opaque and enhance the contrast between the mount and the respective phases when studying the fracture profilometry using an optical microscope. The mounted specimens were first polished using a series of wet SiC polishing papers starting from 240 grit size and ending with 800 grit size papers. The subsequent polishing steps were carried on lapping cloth with diamond suspension as the abrasive media. The polishing was carried out in steps using 9, 6, 3, and 1 μm diamond suspension solutions. The final step involved polishing

using 0.05 colloidal silica solution. Figure 17 illustrates typical polished metallographic surface obtained in this manner without etching.

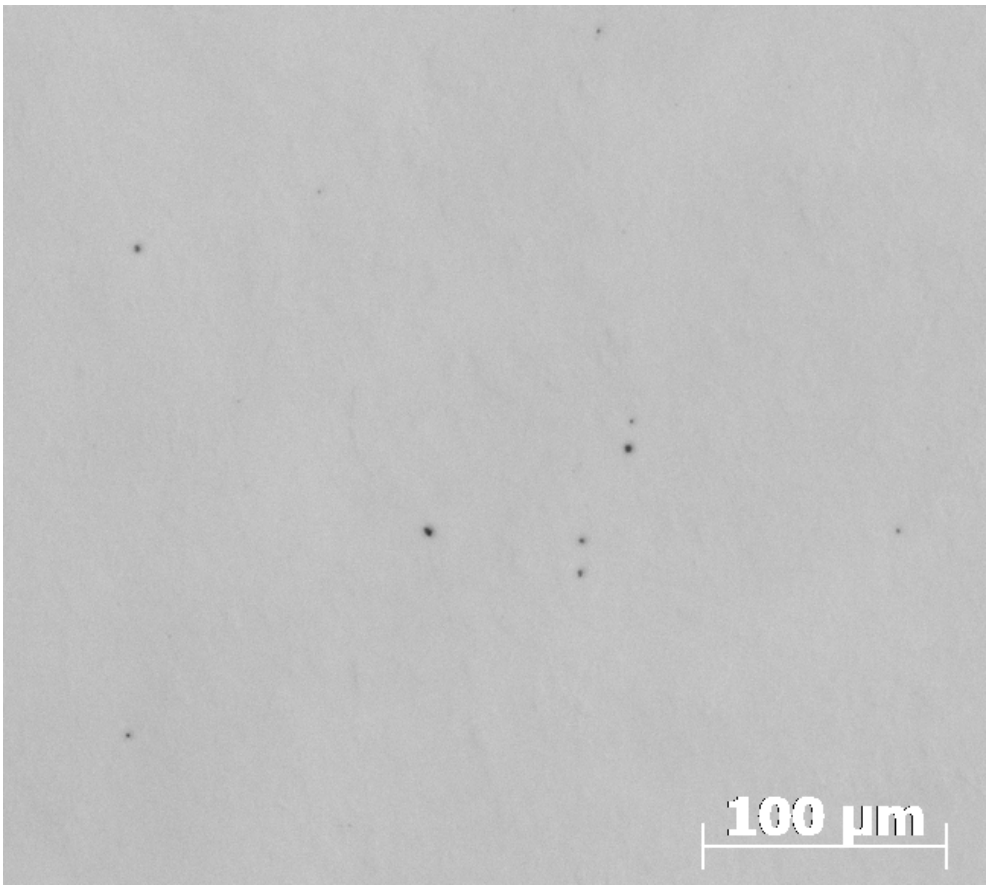

Figure 17: Optical micrograph showing unetched surface of a specimen after polishing

The polished metallographic specimens were etched with using a two-step etching procedure to obtain good contrast between ferrite and tempered martensite constituents. First, the specimens were etched at room temperature in 3% nital solution (3% HNO_3 in ethyl alcohol) for 5 seconds. The specimens were then etched using 10% aqueous sodium metabisulphite ($Na_2S_2O_5$) solution for 28 seconds at room temperature. This etching procedure gives the right contrast between the two phases: nital etch delineates the ferrite

boundaries, and the $Na_2S_2O_5$ etches the tempered martensite dark. The micrographs of the representative microstructures revealed in this manner are given in the next Chapter.

3.4 Digital Image Processing

The microstructures of the etched specimens were observed using an AXIOVISION (Zeiss) optical metallograph connected to a digital image acquisition and analysis computer through a CCD camera. The microscope has programmable automatic specimen stage and auto-focus capabilities. To avoid any edge effects in the estimation of the stereological parameters (see section 2.4 of Chapter II), large number of contiguous microstructural fields were grabbed using a CCD camera attached to the microscope and stitched together to create a high-resolution large-area "montage". The pixel resolution (pixel size) in these montages is 0.1253 microns and the area is 3.28 mm^2. This allows stereological measurements to be made on a large metallographic plane and thus ensuring the results obtained are free from bias and statistically correct. To measure the microstructural parameters, the gray scale images so obtained were first converted to binary images (only white and black) by the process of "thresholding" or segmentation.

3.5 Microstructural Parameters

Once the microstructural images are grabbed and saved in the computer memory, there are available for quantitative stereological measurements. Volume fractions of ferrite and tempered martensite were estimated using stereological point counting technique described in Chapter II. A large number of field of views were taken and a grid was placed on them for point counting. The point counting was performed on the gray

scale images in all three sections- transverse, longitudinal and the planar as shown in Figure 17. The total surface area per unit volume (S_V) of ferrite –martensite interfaces was estimated by performing cycloid line intersection counting technique described in Chapter II. In addition, the mean number of intersections between the interfaces of interest with straight test lines per unit length were also measured along the rolling, transverse, and thickness directions to quantify the anisotropy of the interfaces. The point counting and line intersection counts data were used to validate the segmentation of the gray scale images to obtain the binary images Two-point correlation functions were measured on the segmented images using an in-house C program. The program considers an imaginary rectangle inside the huge montage that is used for calculation, with each side of the rectangle being at least at a distance of the largest distance up to which the two point correlation function is to be measured from the nearest edge. The stereological data obtained in this manner are presented in the next Chapter.

3.6 SEM Quantitative Fractography

The tensile fracture surfaces were analyzed using Hitachi S-4000. The central region (one-third) of each fracture surface was analyzed and images were grabbed in an unbiased manner to make the subsequent calculation based on the SEM images statistically accurate. This was followed for all the samples. The images were then quantified in terms of the % ductile and brittle region. This was again done by the method of point counting using a grid and counting the grid points falling on the dimple regions to give the area fraction of the dimple/ductile fracture taking place. This exercise also gives the amount of brittle fracture taking place through the interface of the ferrite and

martensite. The colonies ferrite-martensite pullouts taking place during the fracture process is also taken into consideration. Since these pullouts are so huge and small in number, their number density can be also estimated manually. The SEM quantitative fractography data are presented in the next Chapter. The data is obtained after using fracture global parameters (that are obtained through profilometry studies) to correct for projection effects in the SEM images. Therefore the results obtained are for the true fracture surface, the details of which have been discussed in the previous chapter.

3.7 Fracture Profilometry

After the SEM analysis, the fractured samples were mounted using cold mounting to protect and preserve the fracture surface during polishing. Since the SEM images were taken of the central one-third region of the fracture surface, the profilometry was also carried out in the same region. In order to reach the central vertical plane of the sample containing the loading axis, the samples were polished and not cut to prevent damage to the profile. Once the central vertical plane is exposed, it is polished using the 0.05um colloidal silica to give the mirror finish and is subsequently etched as mentioned in the section 3.3. Once the fracture profile is obtained it is digitized with help of an in-house C program to give the profile in terms of X and Y coordinates. This is used to calculate the fracture profile through the white or ferrite regions and the path following through the black or martensitic regions. These X and Y coordinates can also be used to input into a computer code to get the fracture roughness parameter (R_S) and structure factor (Ψ) which are in-turn used in SEM–based quantitative fractography measurements.

CHAPTER IV

RESULTS AND DISCUSSION

In this study, the experimental work has been performed on a series of tensile test specimens of a cold-rolled dual phase steel that exhibits significant variability in the uniaxial tensile ductility. The techniques and methodologies utilized in these experiments have been reported in the previous Chapter. In this Chapter, the experimental observations and quantitative data are presented and they are critically analyzed to understand the microstructural origins of the observed variability in the ductility. The data analysis and interpretation lead to important conclusions concerning the relationships between variability in the local microstructure and the observed variability in the tensile ductility. The next section of this Chapter reports the qualitative microstructural observations, and that is followed by quantitative microstructural data, and results of the SEM fractography. The subsequent sections present the analysis and interpretation of the microstructural and fractographic data, which lead to important conclusions of this research. These conclusions are summarized in the next Chapter.

4.1 Qualitative Microstructural Observation

4.1.1 Bulk microstructure

The global microstructures have been characterized in three orthogonal metallographic planes; namely, planar section, transverse section, and longitudinal section (see Figure 16 in Chapter III for orientations of these planes). Figures 18 to 20 depict the representative microstructures in these three metallographic planes.

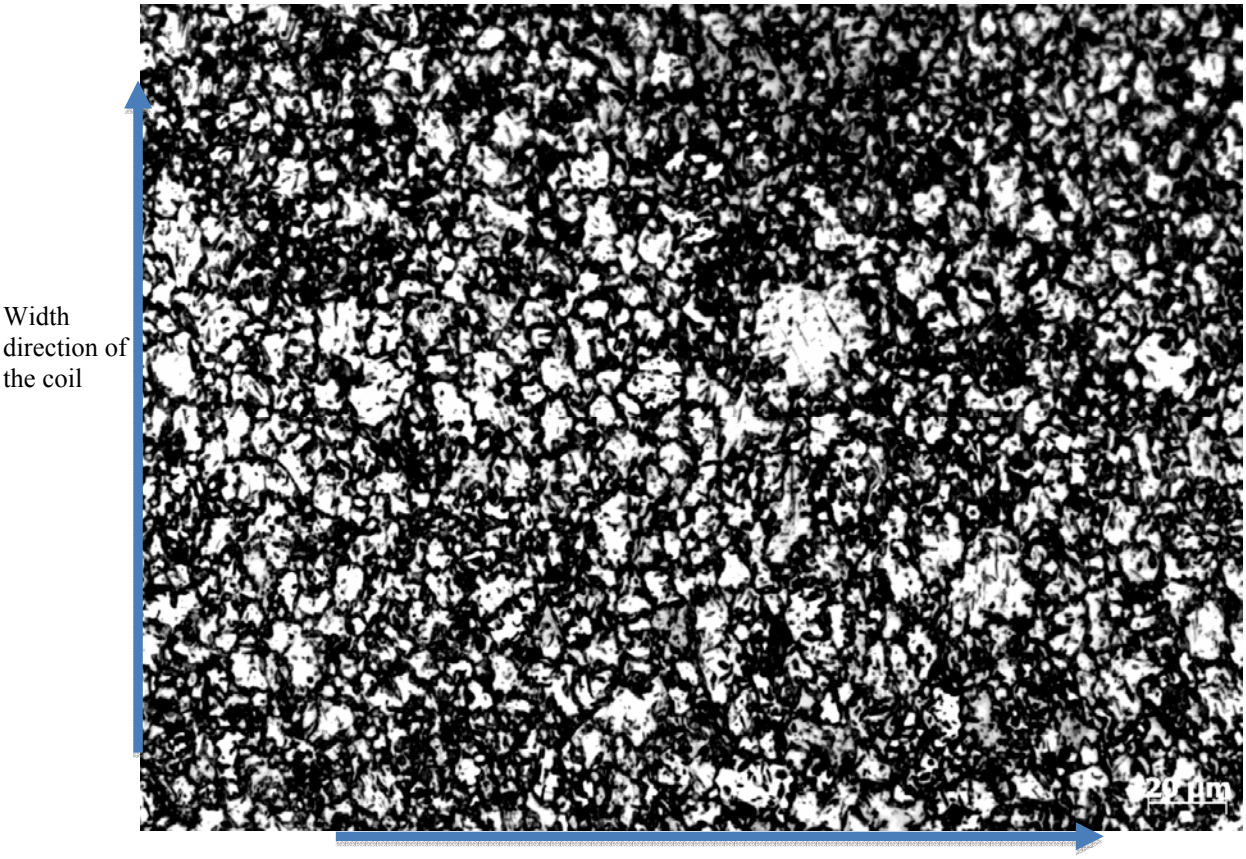

Figure 18: Typical microstructure of the planar section.

Figure 18 shows the planar section of the steel sample. In the micrograph, the bright regions are ferrite, whereas the darkly etched regions are martensite. Observe that, martensite is the continuous phase containing equiaxed dispersed regions of ferrite. Further, in this sectioning plane, the ferrite-martensite interfaces have uniform-random *isotropic angular orientations*. Observe that some ferrite regions enclose small dark martensite (apparently) isolated islands, which are likely to be interconnected with other martensite regions in the third-dimension. The length scale of ferrite regions is of the order of 5 µm in this sectioning plane.

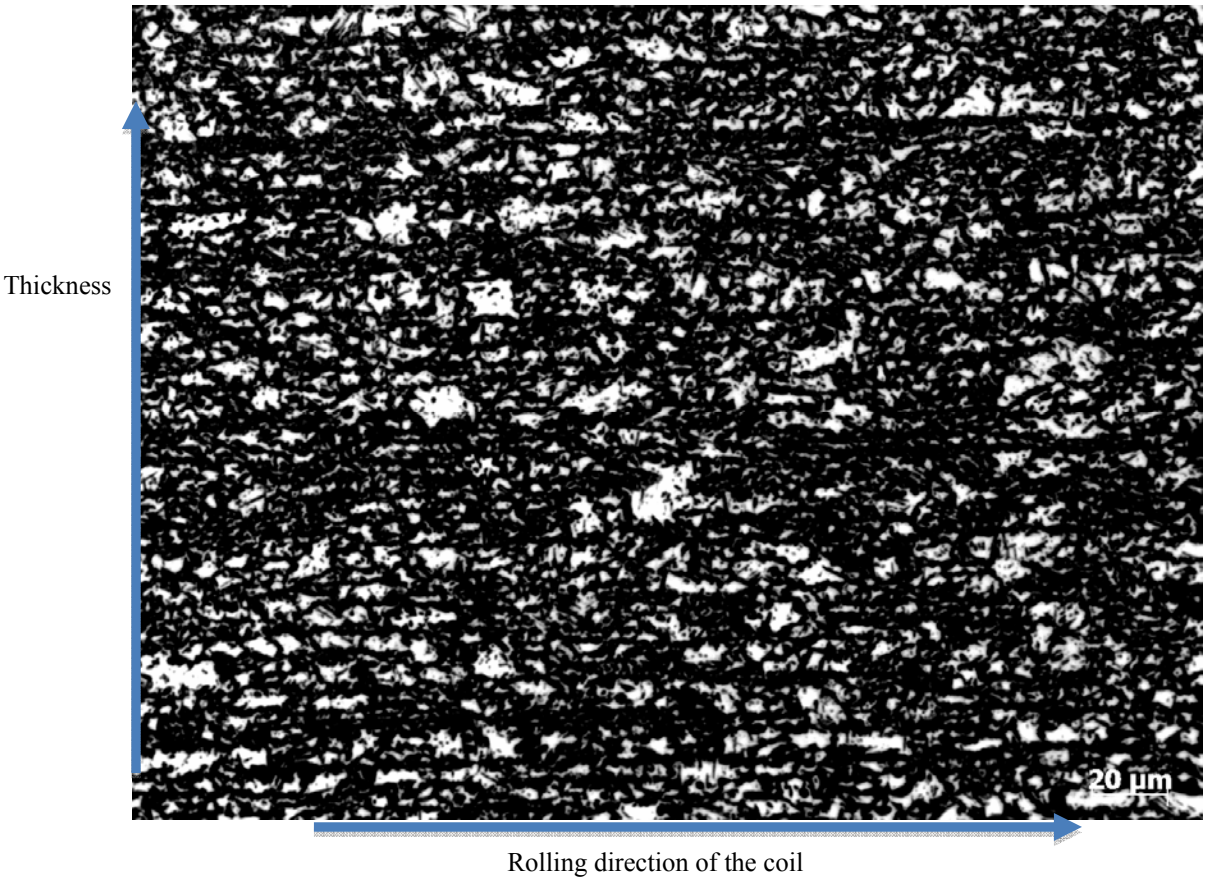

Figure 19: Typical microstructure of the transverse section.

Figure 19 shows the representative microstructure observed in the transverse metallographic section. The X-axis of the micrograph is along the rolling direction and the Y-axis is the thickness direction of the coil. The microstructure appears to be "banded" i.e. due to Mn segregation prominent bands are present along the rolling direction of the coil in the micrographs. The ferrite regions and ferrite-martensite interfaces appear to have preferred orientation along the rolling direction of the coil. Nonetheless, martensite is still the continuous phase as observed in the planar section.

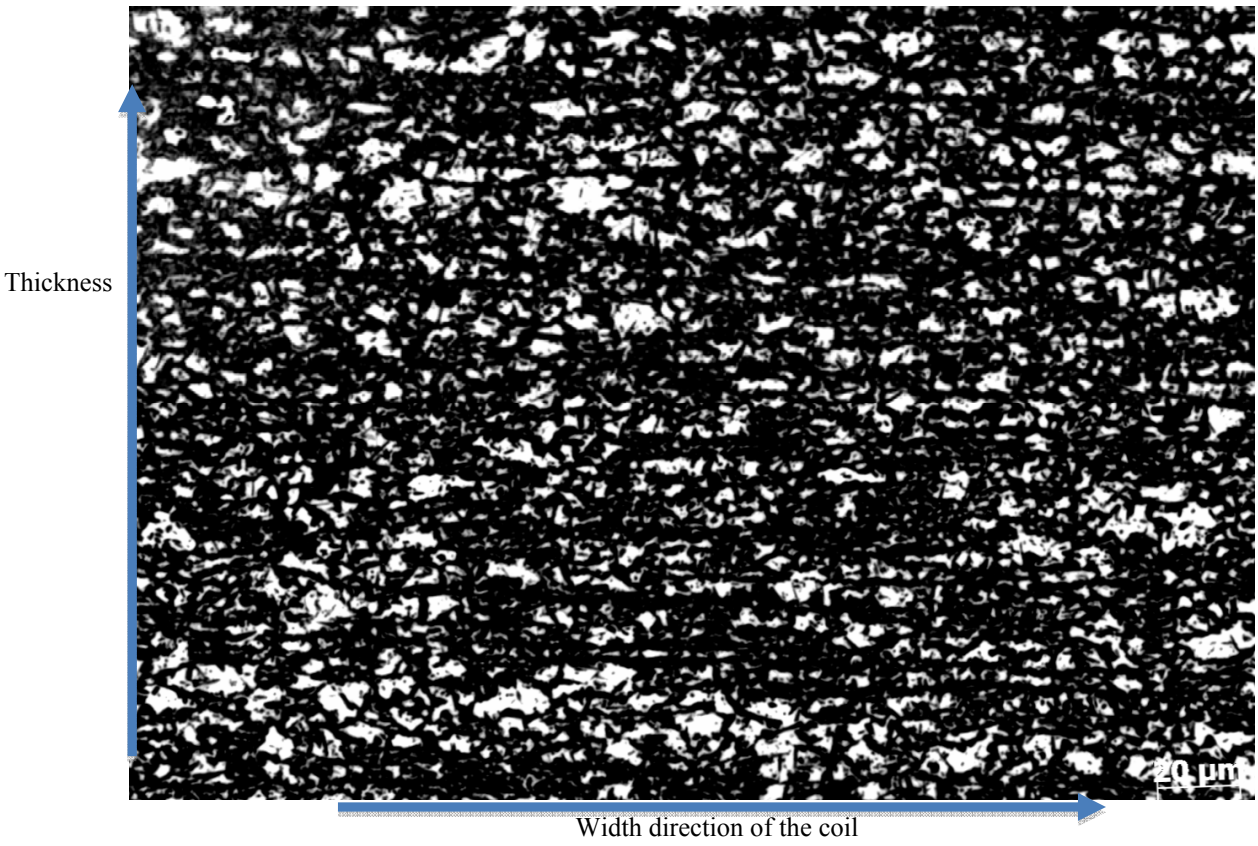

Figure 20: Typical microstructure of the longitudinal section.

Figure 20 shows typical microstructure observed in the longitudinal section cut from the steel coil. In this micrograph, the X-axis is along the width of the coil (or in other words length of the tensile test specimens and loading direction) and the Y-axis is the thickness direction of the coil. The longitudinal section (like the transverse section) also exhibits banding, but in this case, the width direction of the coil is the direction of anisotropy. Further, in this section as well, the continuous phase appears to be martensite. Thus, the longitudinal and transverse metallographic sections exhibit banding and anisotropy, whereas the planar section exhibits isotropic two-dimensional microstructure. Further, due to the high volume fraction of martensite in this dual phase steel, the microstructure

shows islands of ferrite arranged in bands in the topologically continuous phase of black martensite in all three orthogonal metallographic sections. A 3D view of the planes shown in Figure 21 clearly illustrates the ferrite and martensite morphologies.

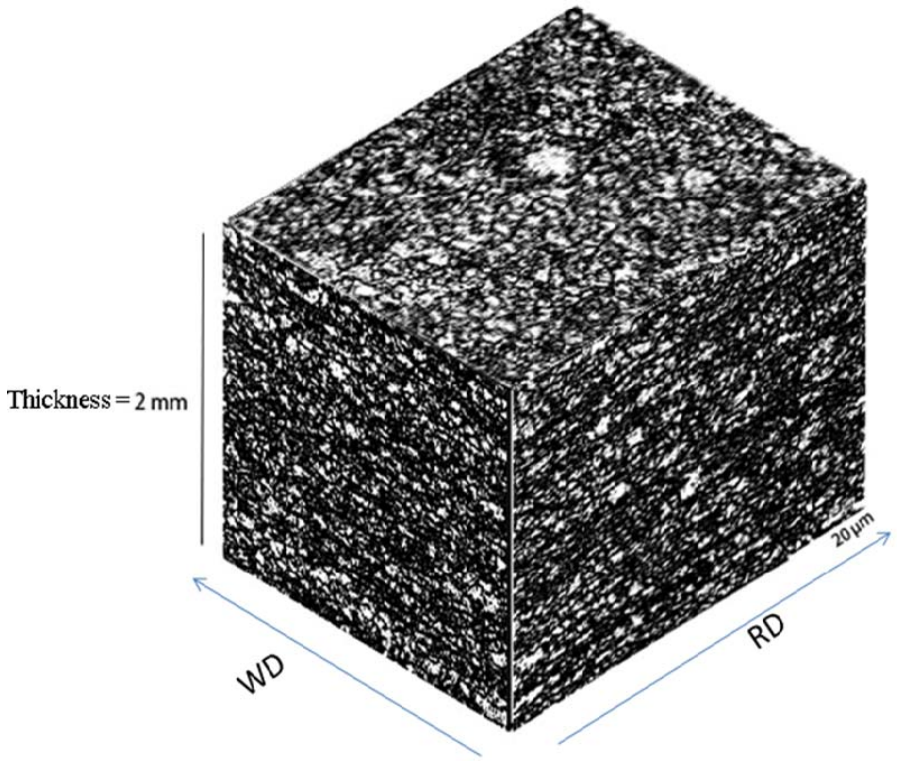

Figure 21: A 3D view of the global microstructure along the three planes illustrating dispersed ferrite islands in the topological continuous phase of black martensite.

4.1.2 Local Microstructure Below Fracture Surface

As explained in Chapter III, the fractured tensile test samples were mounted for profilometry studies and subsequently polished to observe the fracture profiles and local microstructures below the fracture profiles. Figure 22 depicts one such typical local microstructure below the fracture profile/surface.

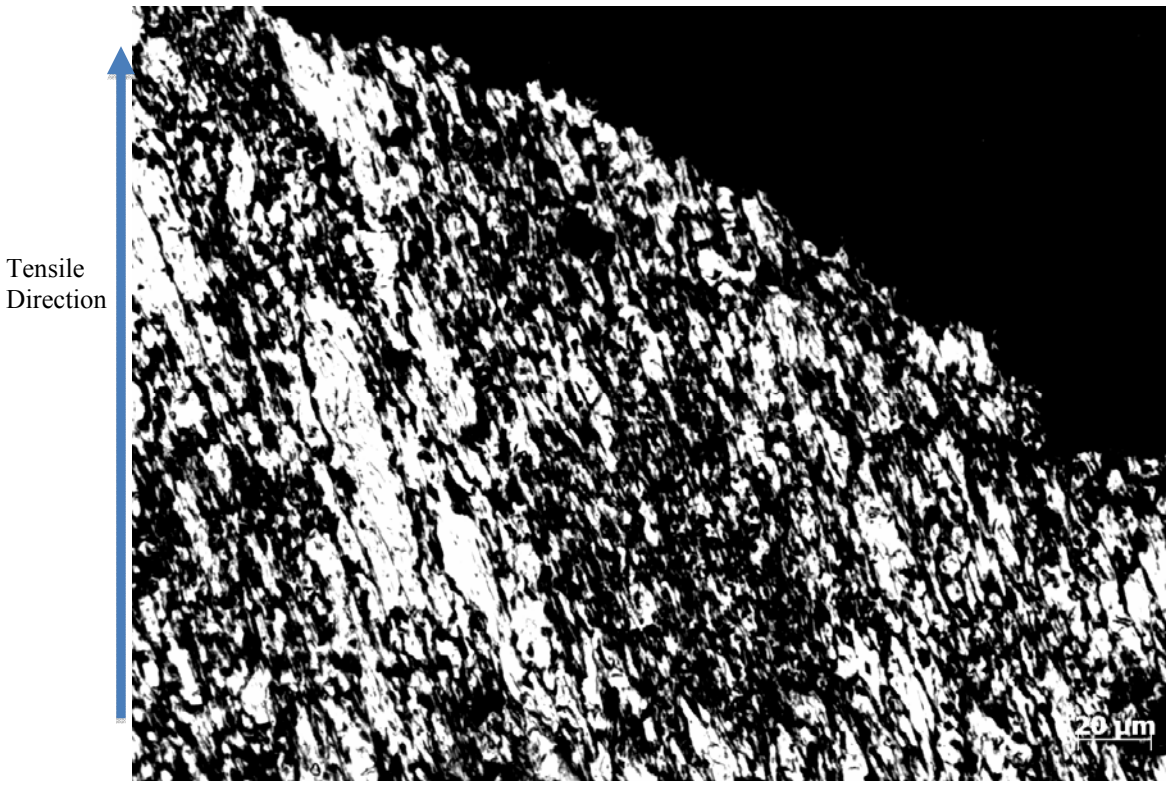

Figure 22: Shows the elongated ferrite islands in the near fracture region.

In this micrograph, the Y-axis is parallel to the loading direction of the tensile test specimen, which is also the width direction of the steel coil; the X-direction is along the rolling direction of the coil. Therefore, in this metallographic plane, the orientation is the same as the planar section (Figure 18) of the coil. Comparison of the local microstructure of the planar section just below the fracture profile observed in Figure 22 with the global microstructure of the planar section in Figure 18 clearly reveals that (i) the local microstructure below the fracture profile is considerably anisotropic whereas the global microstructure is isotropic in the planar metallographic section orientation, and (ii) in the local microstructure below the fracture profile, the ferrite island are elongated and they are oriented roughly at an angle of 45◦ with the loading direction (Y-axis). Figure 36

shows another frame of view clearly depicting the elongation of the ferrite islands along the preferred direction. Going down few frames of view away from the fracture profile in the same mounted steel sample, the microstructure regains its isotropy as shown in the Figure 23.

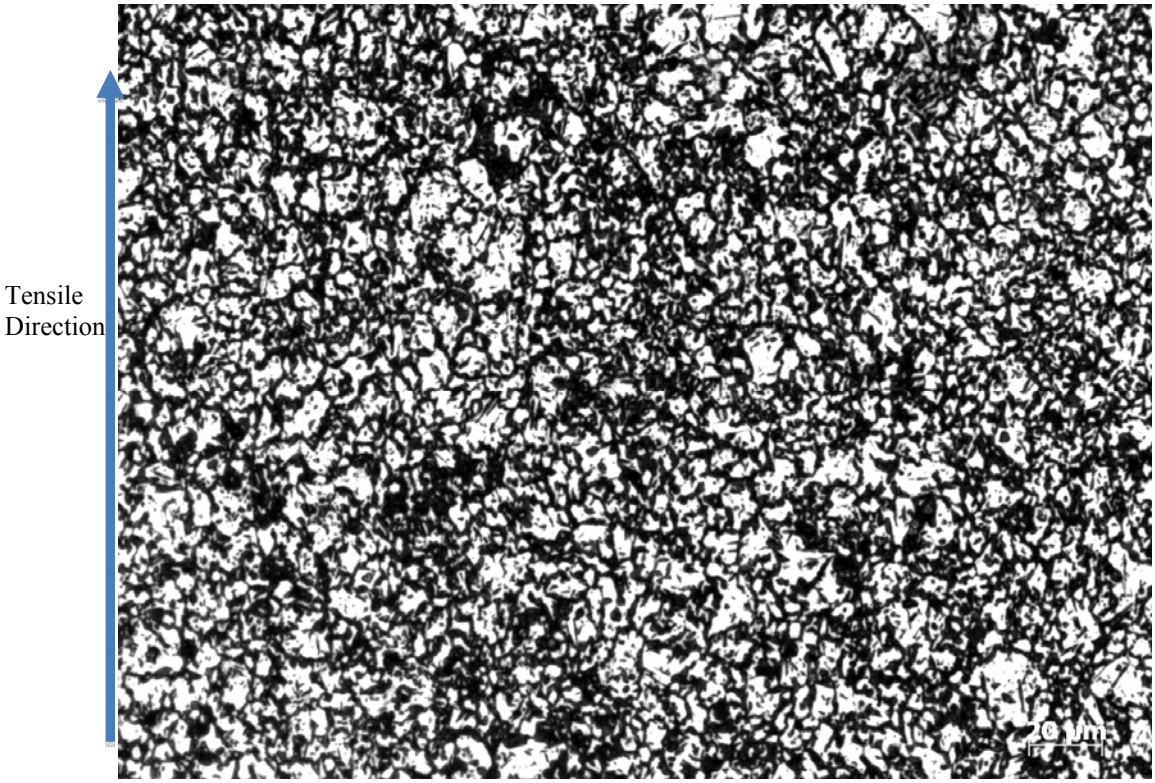

Figure 23: Shows the isotropic ferrite islands in the microstructure away from fracture profile.

These observations reveal that the intense local plastic deformation of the specimen in the vicinity of the tensile fracture surface leads to severe local deformation of the ferrite regions (soft and ductile phase) and rotation of the ferrite-martensite interfaces so that they are aligned roughly along the direction of maximum shear stress (45◦ with respect to the tensile loading direction). Nonetheless, severe local plastic deformation is needed for

this change in the microstructure because the anisotropy and rotation of ferrite-martensite interface is not observed just about 4 field of views below the fracture surface (see Figure 23) where the extent of plastic deformation is only on the order of the global tensile strain. Such anisotropy can affect the evolution of local and global fracture, in particular if the interface fracture is an important fracture micro-mechanism. Rotations of the ferrite-martensite interfaces associated with the tendency to align along the direction of maximum shear stress, *decreases* the total projected area of these interfaces perpendicular to the applied tensile stress direction, and thereby it should decrease the extent of the fracture path along ferrite-martensite interfaces. This can lead to an increase in the total elongation, if the interface decohesion is an important fracture micro-mechanism. In the subsequent section quantitative microstructural fractographic data are utilized to show that this is indeed the case: the projected interfacial area of the ferrite-martensite interfaces in the plane perpendicular to the applied tensile stress direction is indeed lower in the specimens exhibiting high tensile ductility. It must be pointed out that although rotations of brittle inclusions during plastic deformation of wrought non-ferrous alloys [44] and steels have been reported in the literature, to the best of author's knowledge rotations of *ferrite-martensite interfaces* due to intense local deformation of dual phase steels and the likely relationship between such rotations and tensile ductility has not been reported and proposed earlier.

4.2 Quantitative Characterization of Bulk Global Three-Dimensional Microstructure

The mechanical response of the dual phase steels depends on the relative amounts (volume fractions) of martensite and ferrite. Theoretical models reported in the literature predict the effects of volume fractions of ferrite and martensite on the yield stress of the dual phase steels. The finite-elements based numerical computations link the yield stress and ultimate tensile strength of the dual phase steels to the constituent volume fractions assuming a dominant failure mode [9,21,25]. Therefore, volume fractions of ferrite and martensite have been experimentally measured. Total surface area of ferrite-martensite interfaces per unit volume is related to coarseness or fineness and length scale of the dual phase steel microstructure. For given phase volume fractions, a microstructure having higher total interfacial area of the ferrite-martensite interfaces is finer, which is expected to affect the properties such as strength, particularly if the fracture along ferrite-martensite interfaces is an important fracture micro-mechanism. Therefore, the total surface area per unit volume has been experimentally measured in this research. Other microstructural attributes may also influence the fracture sensitive mechanical properties such as ductility and ultimate tensile strength. Two-point correlation function implicitly contains the information about these microstrucutral attributes as well as numerous other microstructural parameters. Consequently, in this research, the two-point correlation functions of bulk microstructure have also been experimentally measured. These experimental data are reported and critically analyzed in the following sub-sections.

4.2.1 Volume Fraction and Surface Area per unit volume

The microstructure of the present dual phase steel contains ferrite islands dispersed in martensite along with small martensitic areas enclosed within the ferrite phase. The volume fractions of the two constituent phases and the total surface area of the ferrite-martensite interfaces per unit volume, S_V were estimated using the technique described in Chapter II. These experimental data are given in Table 4. These data represent the average values obtained from the measurements performed on the three orthogonal metallographic sectioning planes along with the ranges with 95% confidence level. The 'n' value denoted in the table refers to the number of field of views on which calculations were done for each of the dual phase steel specimens.

Table 4

Volume Fraction and Surface area per unit volume between the ferrite and martensite phases in the bulk microstructure of the dual phase steel samples

Total Elongation (%)	Volume Fraction Ferrite Vv (%) (n= 18)	Volume Fraction Martensite Vv (%) (n= 18)	Surface area per unit volume-Sv (/um) (n= 18)
10.1	36.5 +/- 3.02	63.5+/-3.02	0.73+/-0.027
11.9	38.7+/-2.10	61.3+/-2.10	0.80+/-0.03
13.1	35.5+/-2.20	64.5+/-2.20	0.76+/-0.015
14.0	37.3+/-3.10	62.7+/-3.10	0.71+/-0.020
15.8	34.0+/-2.4	66+/-2.4	0.68+/-0.018

Inspection of the data in table 4 reveals that there is no significant specimen to specimen variation in the volume fractions of ferrite and martensite: in all specimens the volume fraction of martensite is in the range 63.5 +/- 2.5 %. Therefore, it can be concluded that the observed variability in the uniaxial tensile ductility (10.1 to 15.8%; more than 50% change) of these specimens cannot be attributed to the specimen to specimen differences in the global volume fractions of the phases. The experimental data on the surface area per unit volume between the two phases also doesn't indicate any particular significant trend from the highest to the lowest ductility samples. Therefore, it can be concluded that there are no significant specimen to specimen differences in the first order bulk global microstructural properties, volume fractions and total surface area of ferrite-martensite interfaces per unit volume. Consequently, the observed variability in the tensile ductility must be due to other microstructural factors.

4.2.2 Two Point correlation function

The two-point correlation function was carried out on the segmented binary images of bulk microstructures. These measurements were performed on the binary microstructures generated from the three orthogonal metallographic planes to estimate the two-point correlation function along the rolling direction, transverse direction, and thickness direction of the specimens. Figure 24 depicts normalized ferrite-ferrite correlation function along the three orthogonal directions for the specimens of 10.1% ductility; the normalization is by the square of the ferrite volume fraction. Observe that all the curves approach the same values as the distance r approaches zero and as r becomes very large (strictly, as r approaches infinity). Nonetheless, there are clear

differences in the three curves at other values of the distance r. These differences are due to the anisotropic orientations of the ferrite-martensite interfaces due the "banding' resulting from Mn segregation. Therefore, the two-point correlation function nicely captures the banding and anisotropy of the microstructure.

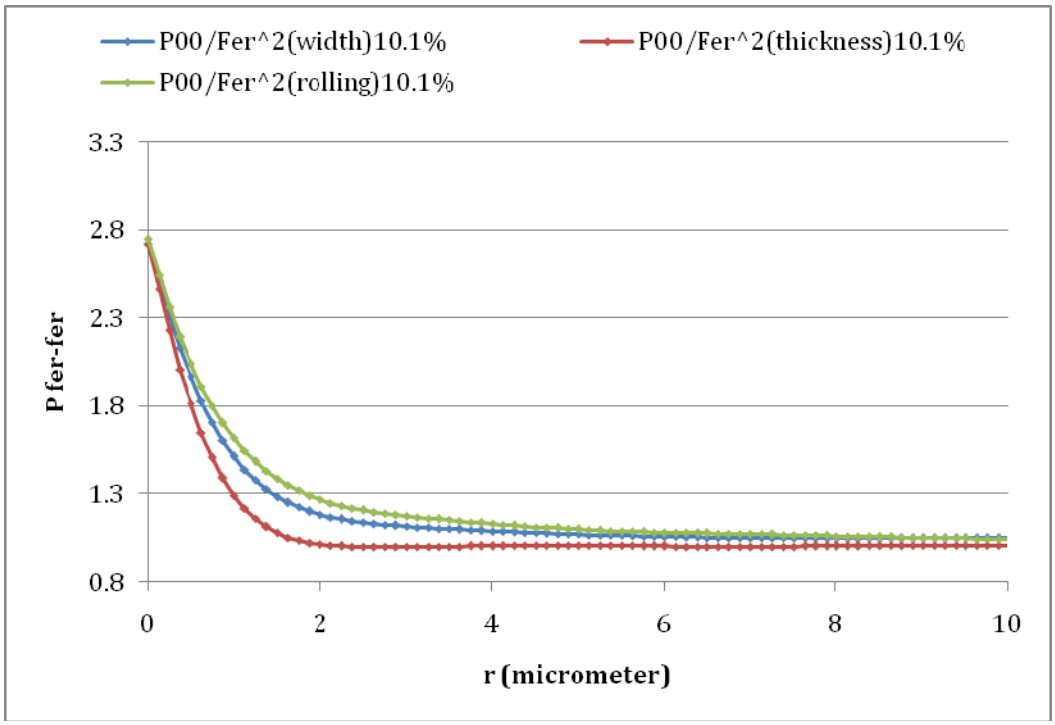

Figure 24: Shows the two-point plots for the lowest ductility steel in the three orthogonal directions.

Note that in Figure 24 although all three curves approach the same value as the distance r approaches zero, the slopes of the three curves as r approaches zero are quite different, which is also due to the anisotropic nature of the microstructure. Figure 25 below shows the two-point plot for the specimen with the highest total elongation 15.8%.

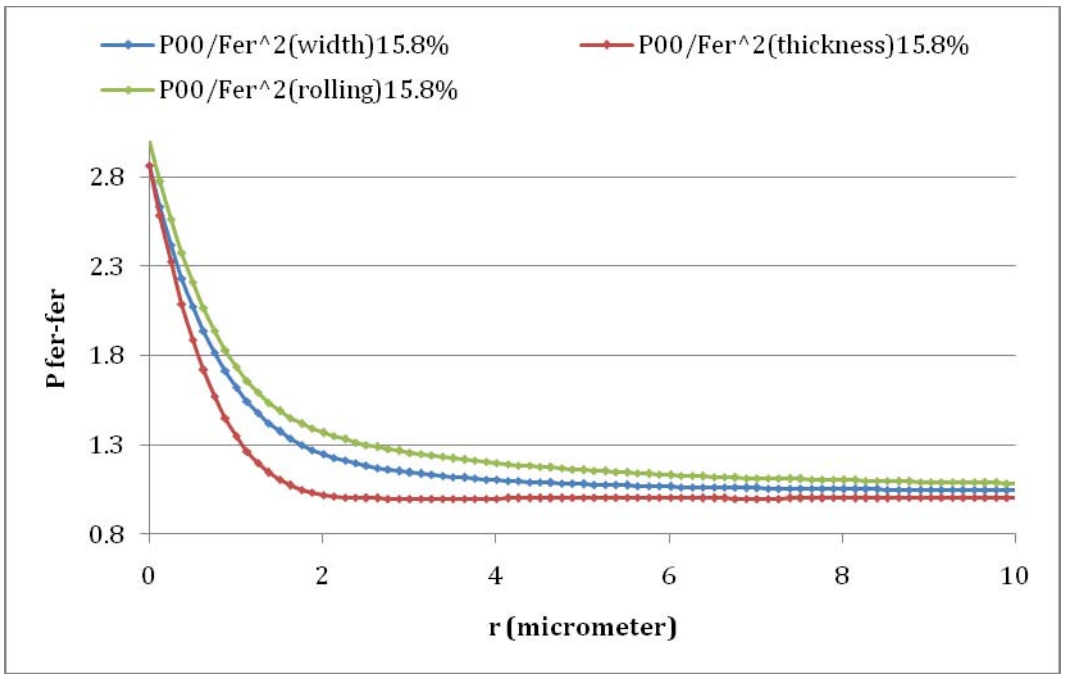

Figure 25: Shows the two-point plots for the highest ductility steel in the three orthogonal directions.

Figure 26, 27 and 28 show a comparison between three different steel samples from the given set.

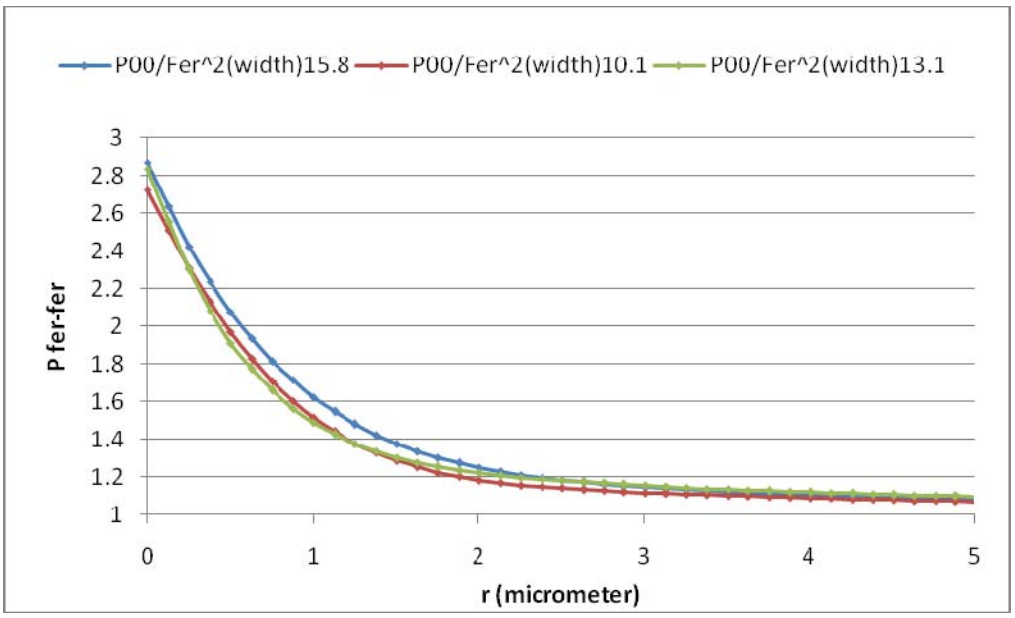

Figure 26: Shows the two-point plots for three dual phase steel samples along the width direction of the coil.

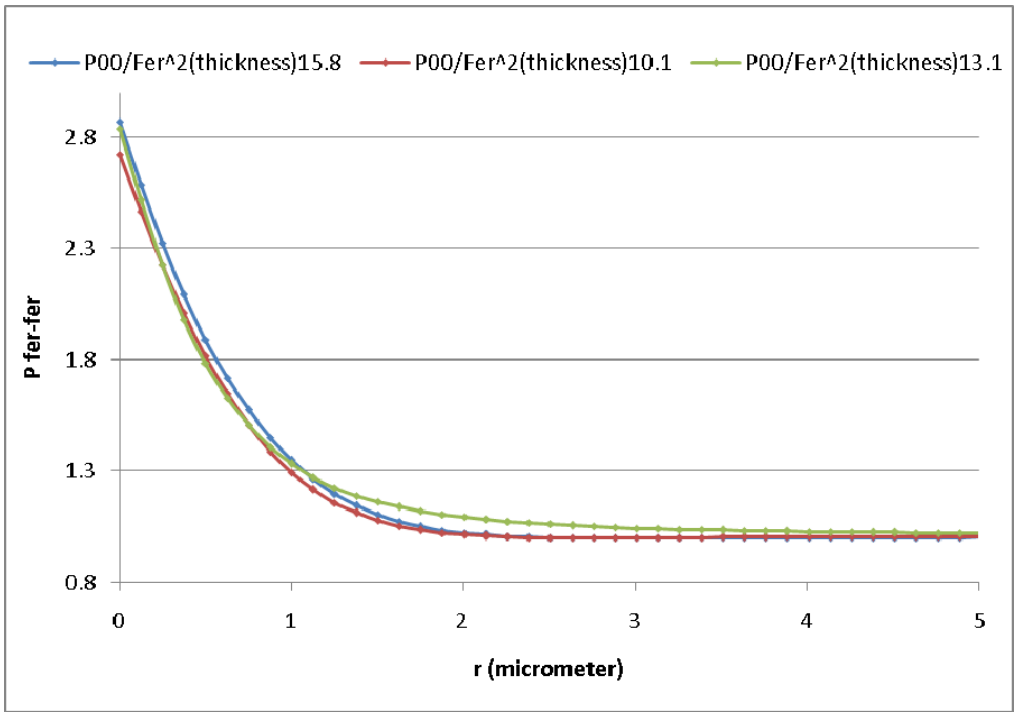

Figure 27: Shows the two-point plots for three dual phase steel samples along the thickness direction of the coil.

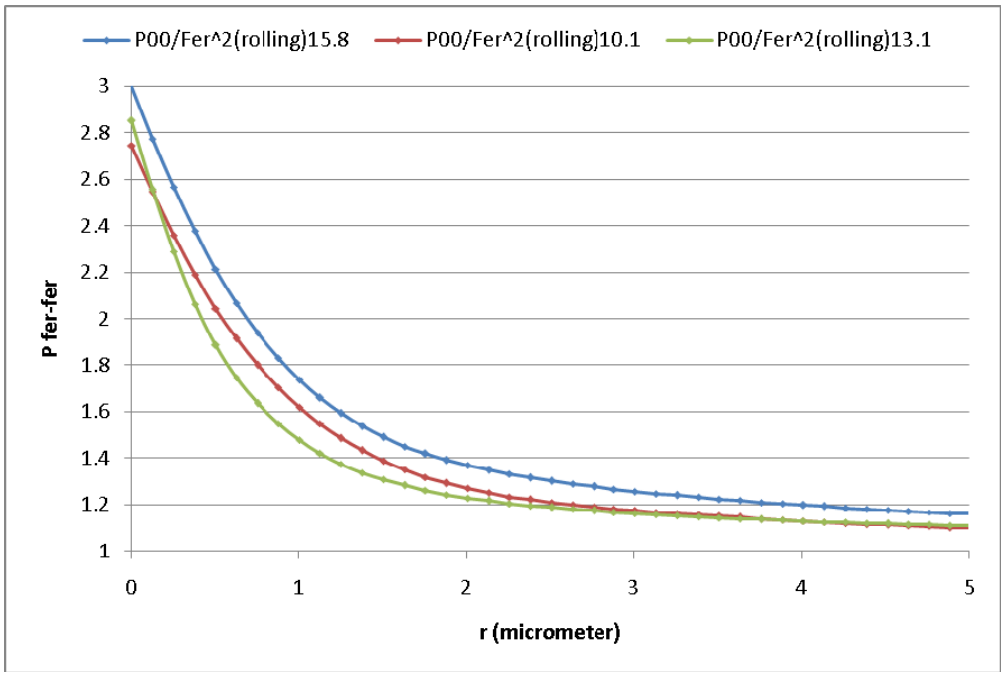

Figure 28: Shows the two-point plots for three dual phase steel samples along the rolling direction of the coil.

Here the two-point correlation functions of the three samples with total elongation of 10.1%, 13.1% and 15.8% are compared along the three orthogonal directions. The two point plots for the three samples show small variation when compared in a specific direction, which is probably due to minor variations in the nature of banding from one specimen to another. Nonetheless, the major differences in the ductility of these specimens are not likely to be due to such minor microstructure variations. Therefore, it can be concluded that the there are no significant specimen to specimen variations in the bulk global microstructures of the specimens studied. Therefore, the observed variations in the ductility are likely to be due to local variability in the microstructure in each specimen.

4.3 Quantitative Characterization of Local Microstructure Below Fracture Surfaces

Qualitative observations of local microstructure below the fracture profiles in the planar orientation metallographic sections reveal that (i) the local microstructure below the fracture profile is considerably anisotropic, whereas the global microstructure is isotropic in the planar metallographic section orientation, and (ii) in the local microstructure below the fracture profile, the ferrite island are elongated and the ferrite-martensite interfaces are oriented roughly at an angle of 45◦ with the loading direction. If ferrite-martensite interface decohesion is an important fracture mechanism, then the ferrite-martensite interface segments perpendicular to the applied tensile stress direction are more likely to fracture than those parallel to the applied tensile stress direction. Therefore, the variability in the fracture sensitive properties such ductility may be partly due to the variations in the *local anisotropy* of ferrite-martensite interfaces. Interestingly, the component of the interfacial surface area in the three-dimensional microstructure oriented perpendicular to the applied tensile stress direction can be estimated in a straightforward manner by using the following general stereological relationship [11,12].

$$I_V = (P_L)_{II} \tag{16}$$

In equation 16, $(P_L)_{II}$ is the number of intersections of ferrite-martensite boundaries with test lines oriented parallel to the applied tensile stress direction per unit test line length, and is the projected area of the ferrite-martensite interfaces perpendicular to the applied stress direction per unit volume of microstructure, which is precisely the component of the ferrite-martensite interfacial area perpendicular to the applied stress. The figure below explains the geometric reasoning at the root of equation 16.

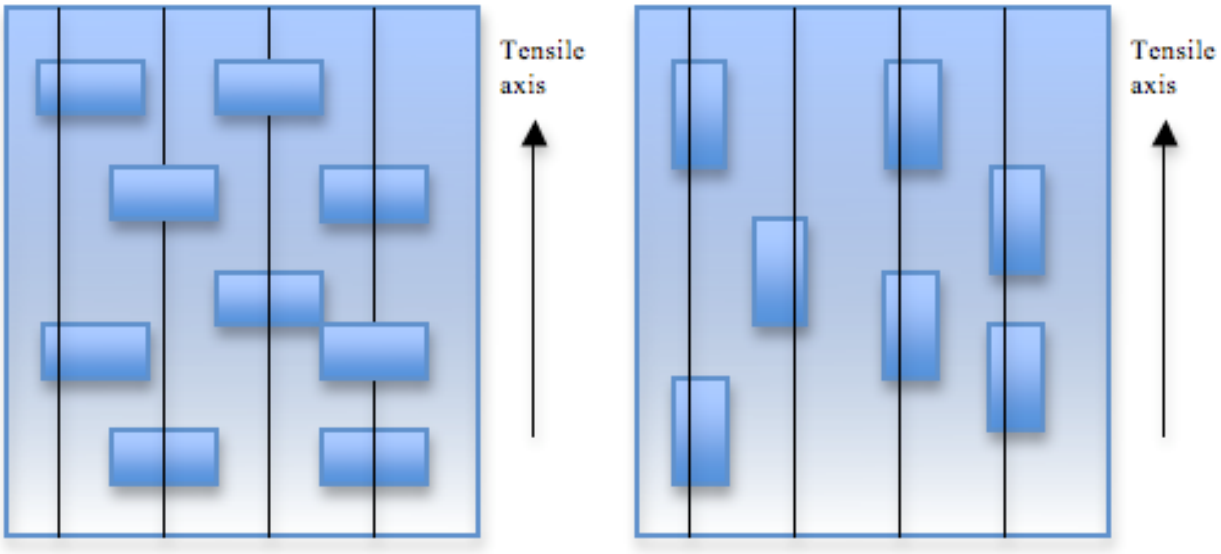

Figure 29: A schematic showing the use of the interface-orientation parameter **Iv** to estimate the exposed ferrite-martensite interfacial area.

As shown in the figure 29 a) the number of intersections of the four test lines with the boxes are 18 while that in figure b) is 14. The figure a) has boxes with their length perpendicular to the direction of the test line and thereby increasing the chances of intersection with the test lines. In figure b) the boxes are arranged with their length oriented along the test line direction and thereby having a total intersection count as 14. This example is synonymous with the ferrite islands being oriented with respect to the test lines that are placed on the microstructure parallel to the tensile axis. Greater the number of intersections per unit test line length, greater is the angular orientation of the ferrite islands or in other words the ferrite-martensite interface with the tensile axis.

The measurements of $(P_L)_{II}$ were performed on the local microstructure just below the central region of the fracture profiles, local microstructure just below end region of the fracture profile, and in the microstructure substantially away from the fracture profile in the planar metallographic sections. These data are reported in Table 5

along with the possible range of values for each specimen. The 'n' value denoted in the table refers to the number of field of views on which calculation were done for each specimen.

Table 5

Interfacial-orientation parameter I_V calculated for near fracture regions and the bulk microstructure away from the fracture profile.

Total Elongation (%)	Near-Fracture Region (Center) $[I_V]_{central}$ (n= 20)	Near-Fracture Region (end) $[I_V]_{end}$ (n= 20)	Bulk microstructure away from the fracture profile $[I_V]_{global}$ (n= 20)
10.1	0.18+/-0.013	0.21+/-0.02	0.26+/-0.033
11.9	0.16+/-0.018	0.2+/-0.022	0.28+/-0.024
13.1	0.15+/-0.02	0.19+/-0.018	0.26+/-0.019
14	0.15+/-0.012	0.18+/-0.015	0.3+/-0.028
15.8	0.14+/-0.015	0.16+/-0.02	0.27+/-0.017

Inspection of Table 5 reveals the following.

- As the tensile ductility increases, the component of total ferrite-martensite interfacial area per unit volume in the local microstructure below central region of the fracture profile $[I_V]_{central}$ as well as the corresponding value near the end of fracture profile $[I_V]_{end}$ *decrease* systematically. Therefore, there is a strong inverse correlation between the magnitude of the component of ferrite-martensite total interfacial area perpendicular to the loading direction in the vicinity of the

fracture surface and the tensile ductility. Fracture along the ferrite-martensite interfaces is an important fracture mode, and the *variations in local* ferrite-martensite total interfacial area perpendicular to the loading direction in the vicinity of the fracture surface are responsible for the observed variability in the ductility. This is discussed in detail in section 4.4.

- In all specimens, the $[I_V]_{end}$ is higher than $[I_V]_{central}$ indicating that there is *less* deformation of ferrite regions and more rotations of ferrite-martensite interfaces in the regions experiencing triaxial stress state as compared to the regions in the center where uniaxial stress state prevails.
- In all specimens, the component of total ferrite-martensite interfacial area per unit volume in the bulk global microstructure away from fracture surface $[I_V]_{global}$ is higher than corresponding values in the vicinity of the fracture surface clearly demonstrating reorientation and rotation of the ferrite-martensite interfaces in the vicinity of the fracture surface due to severe local plastic deformation due to strain localization at the neck region.
- There is no specimen to specimen *systematic* variation in $[I_V]_{global}$ that can be correlated with the variability in the tensile ductility, which further confirms that the representative global microstructure is statistically similar in all specimens, and therefore, it is not the cause of the observed variability in ductility.

The unbiased stereological I_V data reported in Table 5 strongly indicates that the decohesion at the ferrite-martensite interfaces is very likely to be a dominant fracture mechanism, and *local variations* in the total area of these interfaces contributes substantially to the observed variations in the tensile ductility. If this hypothesis is

correct, then (i) the area fraction of the fracture surfaces generated by ferrite-martensite interface decohesion must be significant and it should exhibit an inverse correlation with the ductility, and (ii) a substantial length fraction of fracture profiles must be along these interfaces. Quantitative SEM fractographic and profilometric measurements needed to test the hypothesis are reported in the subsequent sections.

4.4 Quantitative Fractography

Fracture surface is the most biased sample of the three-dimensional microstructure because it preferentially goes through those microstructural features that are actively involved in the local and global fracture processes. Further, different fracture modes/mechanisms lead to distinctly different local fracture surface topography. Therefore, roles of local microstructure and fracture micro-mechanisms in the generation of fracture can be quantified via estimation of (i) extent of fracture paths through different phases/constituents, and (ii) extent of fracture path generated by different fracture mechanisms. In the present research, these attributes have been estimated by utilizing the data from SEM quantitative fractography and fracture profilometry.

4.4.1 SEM Quantitative Fractography

The SEM fractographs of the tensile fracture surfaces reveal three types of local fracture topographies, namely, the fracture segments generated due to classical ductile dimple fracture (see Figure 30), the fracture segments generated due to pull-out of packets of ferrite-martensite colonies containing several laths/platelets (see Figure 31) involving interface decohesion, and the fracture surfaces generated due to decohesion of

individual segment ferrite-martensite interfaces (see Figure 32) that do not involve pull-outs.

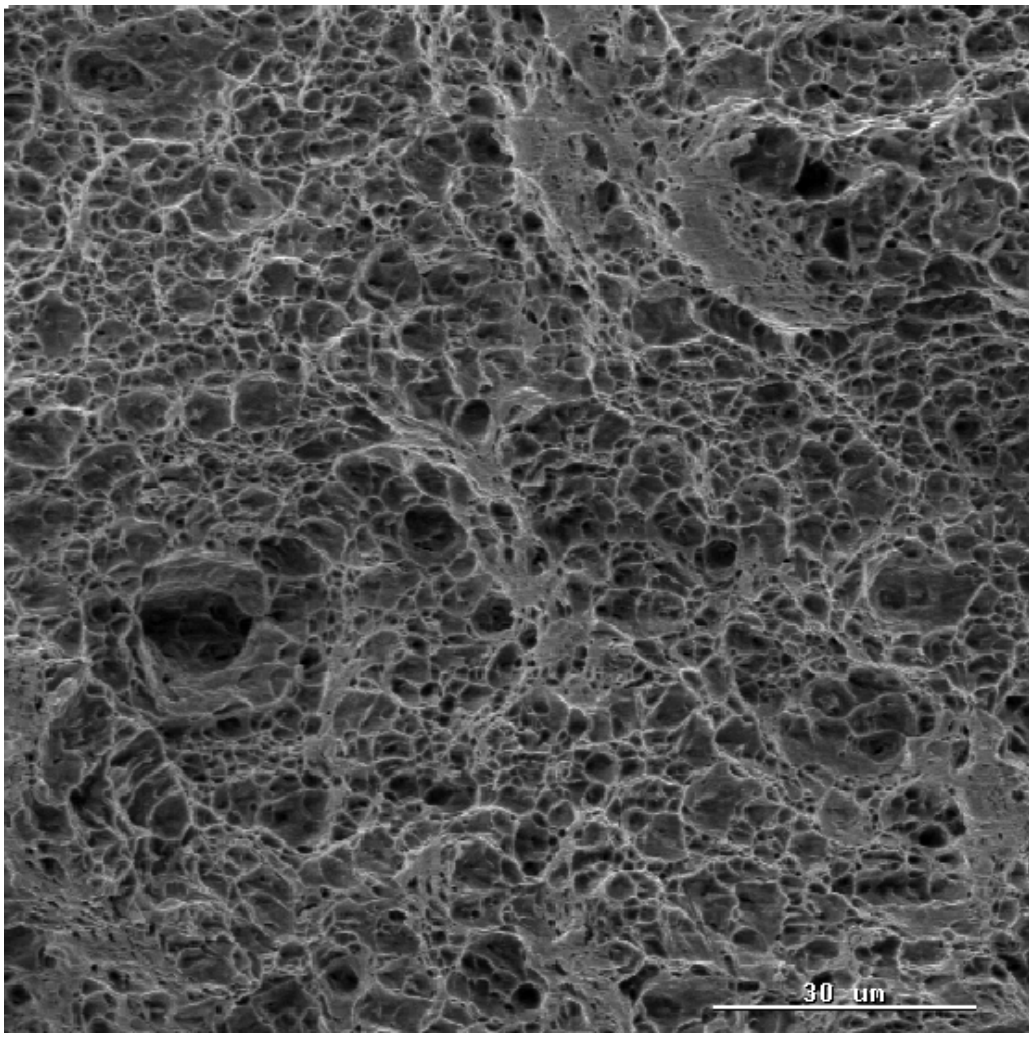

Figure 30: Tensile fracture surface of the highest ductility sample showing dimple ductile regions.

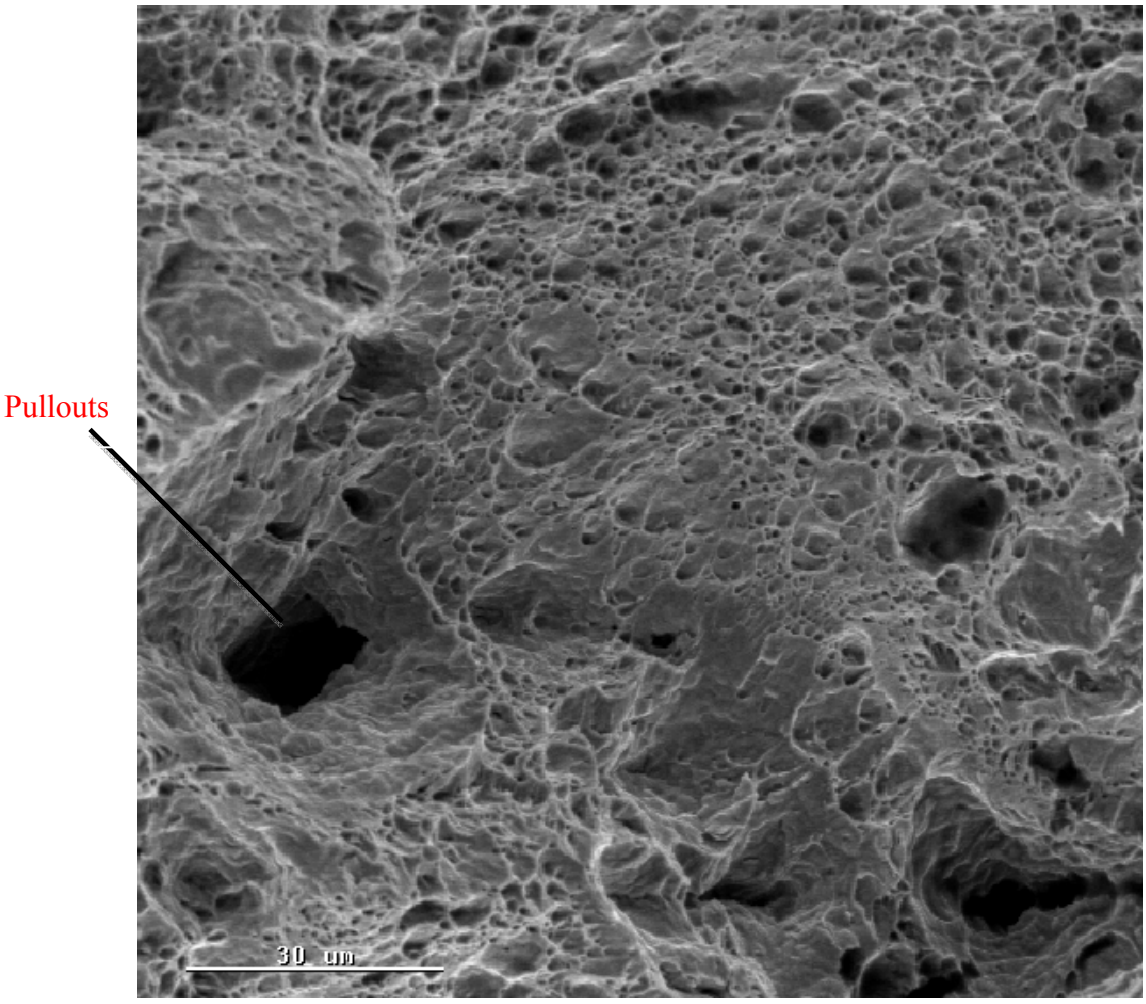

Figure 31: Tensile fracture surface of the lowest ductility sample showing pullouts.

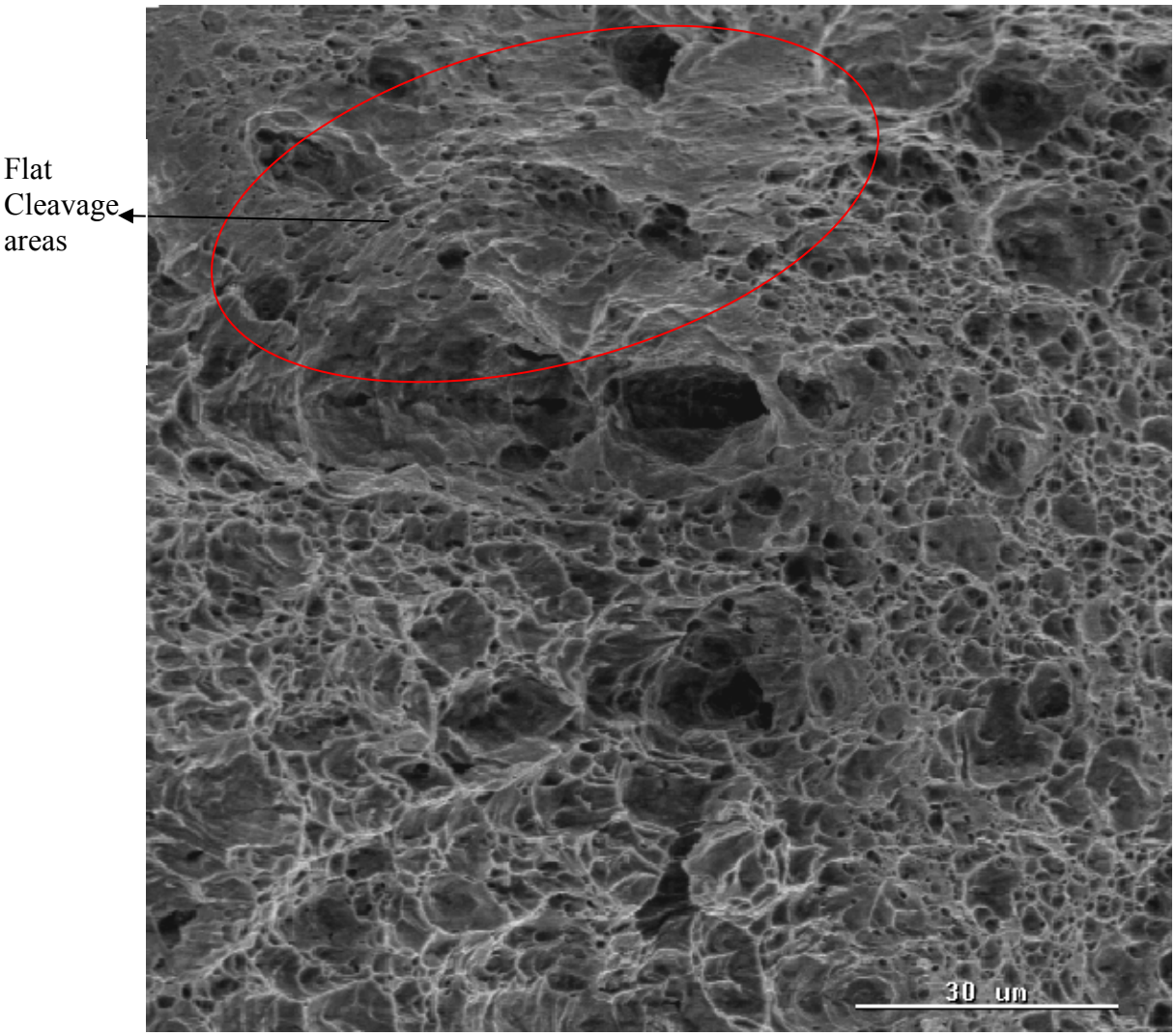

Figure 32: Tensile fracture surface of the lowest ductility sample showing flat interface areas.

The large martensitic pullout regions are generated due to the non-uniformity of strain distribution at the ferrite-martensite interface. Though the martensite in the present grade of steels is imparted considerable amount of ductility by the various chemical and heat treatment processes as mentioned in the previous chapters, incompatibility in deformation between the two phases does exist in areas of large martensitic packets surrounded by ferrite. It is in these interfacial areas that due to significant strain fluctuation decohesion takes place leading to the whole martensitic area along with

ferritic regions being rooted out. Clearly, such pull-outs have deleterious effect on the fracture sensitive properties like ductility. To examine the effect of the pull-outs on the variability in the tensile ductility, the number of ferrite-martensite colonies pulled out *per unit area of the SEM images* were measured. Further, the area fraction of dimpled fracture regions and interface fraction regions *in the SEM images* were also measured for the same purpose. These measurements were performed using the unbiased stereological and fractographic techniques described earlier. These data are reported in Tables 6 and 7. Inspection of these data clearly reveals that there is a strong correlation between the tensile ductility and these parameters. The number density of martensite packet pull-outs is *higher* in the specimens having *lower* tensile ductility. Further, the area fraction of ferrite-martensite interface fracture is also higher in the specimens having lower tensile ductility. To establish unbiased quantitative correlations the corresponding parameters *per unit area of the fracture surface* are needed, which can be calculated if the fracture surface roughness parameters are known [42]**.** The number of pull-outs of ferrite-martensite colonies *per unit area of the fracture surface*, N_F , number of these pull-outs *per unit area of SEM image*, N_S, and the global fracture surface roughness parameter R_S are related as follows.

$$N_F = N_S / R_S \tag{17}$$

The true area fraction of the ferrite-martensite interface fracture in the global fracture surface A_F is related to the area fraction A_S of the interface fracture in the SEM image as follows.

$$A_F = A_S [R_i / R_S] \tag{18}$$

In equation 18, R_i is the roughness parameter for the interface fracture segments. It is impossible to obtain the fracture roughness parameter for the interface fracture mode as the roughness parameter obtained through profilometry studies by measuring the profile length through a given phase is inclusive of the fracture path passing through that particular phase and through the interface. Therefore the maximum information which can be obtained through profilometry studies is the area fraction of the ferrite-martensite interface in the SEM projected images. Even though the values represent the area fraction on the SEM image, with the roughness parameter essentially being the same, the given trend does represent the *true trend* of the area fraction on the fracture surface. The fractographic parameters calculated in this manner are reported in Table 6 and 7. In Table 6, the area fraction of the interface fracture regions is inclusive of the flat, smooth cleavage areas along with the colonies of ferrite-martensite pullouts. The ranges with 95% confidence level are reported.

Table 6

Area fraction of the features in the SEM image for the given set of dual phase steel samples.

Total Elongation (%)	Ductile fracture area fraction of the SEM image (%) (n= 12)	Interface fracture area fraction of the SEM image (%) (n= 12)
10.1	54.1+/- 3.13	45.9+/- 3.13
11.9	58.7+/- 4.27	41.3+/- 4.27
13.1	68.4+/- 3.90	31.6+/- 3.90
14.0	69.1+/- 2.60	30.9+/- 2.60
15.8	71.8+/- 4.01	28.2+/- 4.01

Table 7

Number of pullouts per unit area of the SEM image and per unit area of the fracture surface for the set of dual phase steels samples.

Total Elongation (%)	No. of pullouts per unit area of SEM image Ns ($*10^{-5}$)	No. of pullouts per unit area of fracture surface N_F ($*10^{-5}$)
10.1	12	7.5
11.9	12.5	7.3
13.1	8	4.7
14.0	7	4.1
15.8	6	3.5

Clearly, the data in Tables 6 and 7 reveal interesting trends. The true number density of the packets of ferrite-martensite colonies pulled out from the fracture surface is lower for the specimens having high tensile ductility. Likewise, the true fracture area fraction of the ferrite-martensite interface fracture is lower in the specimens having high tensile ductility. The strong quantitative correlations are also represented in the plots of number density of pull-outs versus tensile ductility and area fraction of interface fracture versus tensile ductility shown in Figures 33 and 34.

a)

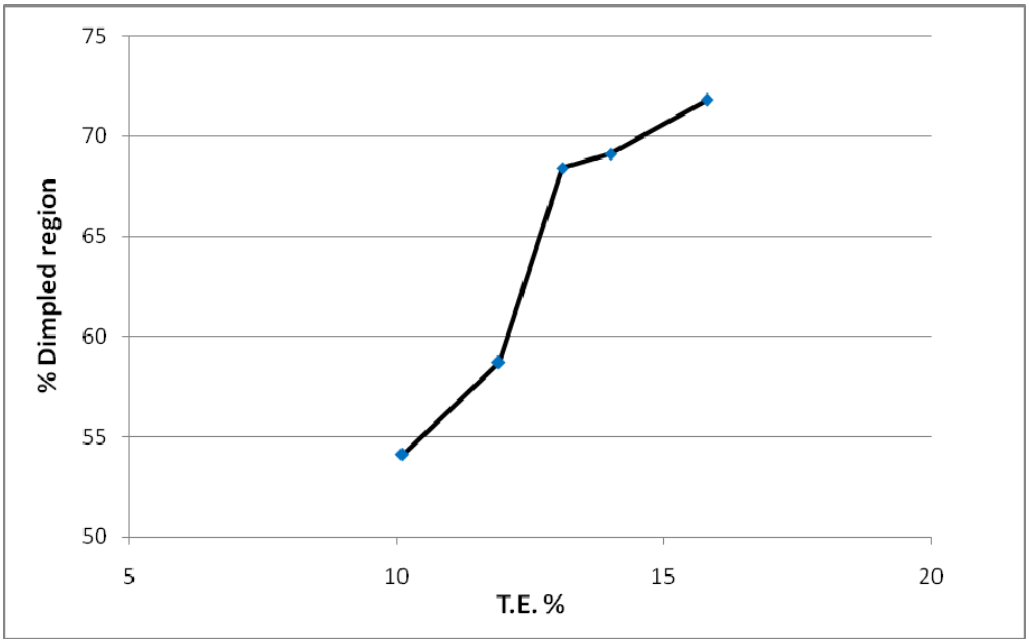

b)

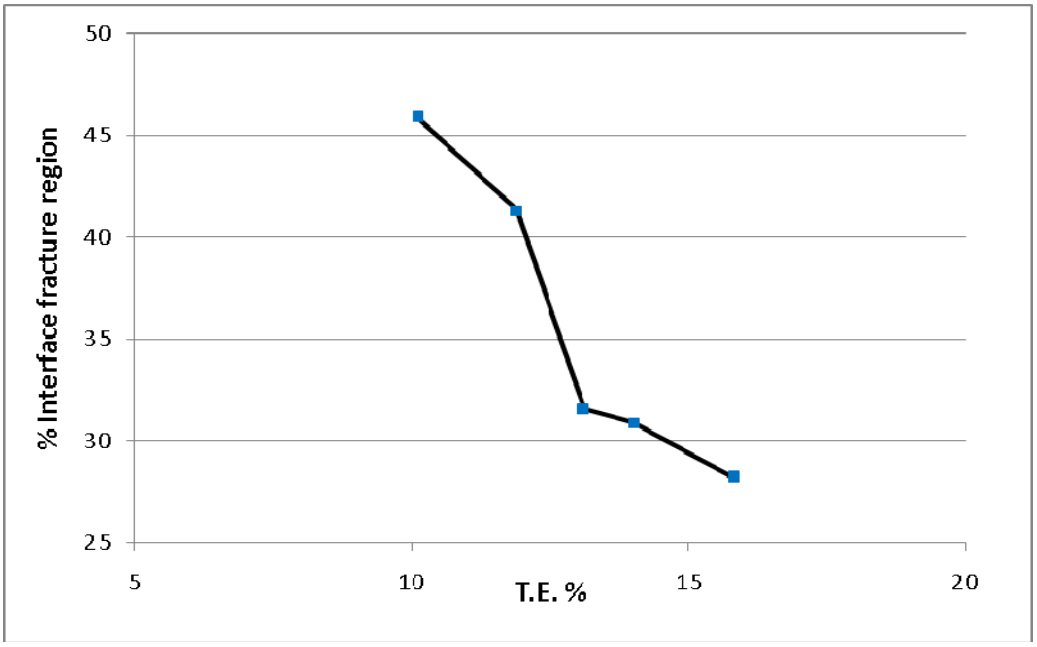

Figure 33: Shows the total elongation of the dual phase steel specimens varying with: a) the % dimple area on the SEM image b) the % Interface fracture area on the SEM image.

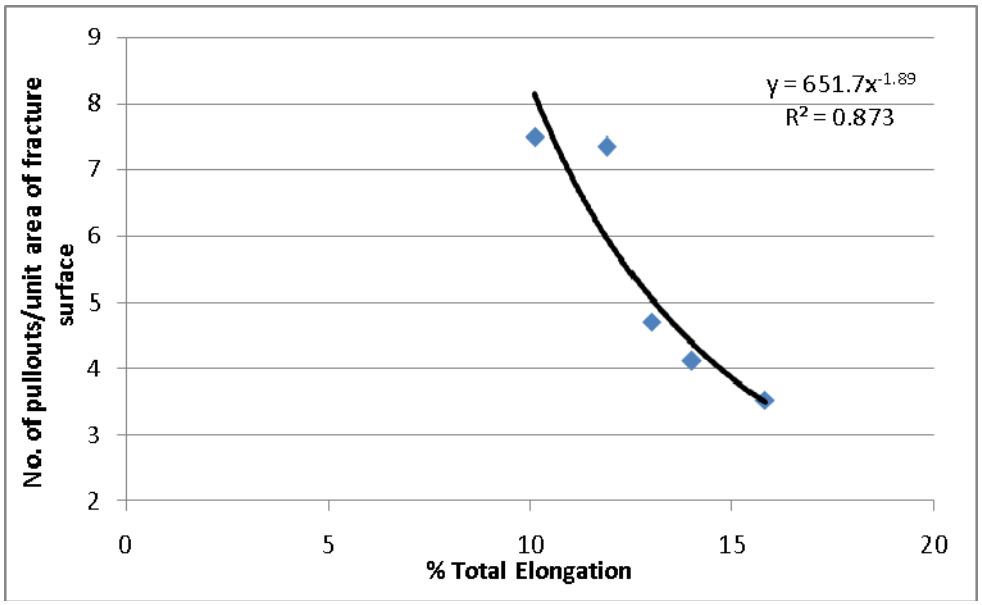

Figure 34: Shows the total elongation of the dual phase steel specimens varying with the number of pullouts on the fracture surface.

These strong quantitative correlations substantiate the claim that non-uniformity in strain distribution and the incompatible deformation between the two phases is one of the prime reasons for variability on a microstructural level. Lesser the number of pullouts on the fracture surface more is the delay in fracture corresponding to an increase in the ductility of the samples.

The *average size of the dimples* on the tensile fracture surface has been estimated using the methodology described in Chapter II. The true average size of the dimples is specified in terms of their average area in the fracture surface. Here the measurements for mean dimple size were carried out in areas where the whole fracture surface consisted of ductile dimple fracture regions as mentioned in Chapter III. Table 8 presents the average dimple size data. Observe that the mean dimple size shows small variation with the tensile ductility. This suggests the higher tensile ductility is not due to larger extent of the plastic deformation surrounding existing micro-voids. This is in sync with the fact that

the tensile ductility variability induced in the specimens is due to the microstructural processes taking place *after* the onset of necking. The uniform elongation of the specimens (in Table 3) shows less variability as compared to the variability in the total elongation. This is also explained by the ultimate tensile strength (UTS) values of the set of specimens, which show low variability. In Table 8 ranges are mentioned along with value of 'n' representing the number of grids/field of views used to calculate the dimple size for each specimen.

Table 8

Average size of the dimples in the SEM image and the true average size in the fracture surface for the set of dual phase steels samples.

Total Elongation (%)	Avg. size of the dimples in the SEM image (um^2) (n= 18)	Avg. size of the dimples in the fracture surface (um^2) (n= 18)
10.1	24.9 +/- 1.13	39.8+/- 1.8
11.9	22.6 +/- 1.72	36.2+/- 2.75
13.1	25.9 +/- 2.10	44.03+/- 3.36
14.0	21.3 +/- 1.08	36.2+/- 1.70
15.8	22.7 +/- 1.40	38.59+/- 2.24

4.4.2 Quantitative Fracture Profilometry

Figure 36 shows the microstructure of dual phase steel in the vicinity of the fracture profile. Figure 22 in section 4.1 shows a similar micrograph. Figure 35 shows the

fracture profile in the unetched condition and figure 36 shows the fracture path passing through the different phases after etching. To quantitatively determine the fraction of fracture profile length through ferrite and martensite constituents and along the ferrite-martensite interfaces, the fracture profiles were traced using an in-house C program which gives the X and Y coordinates of the fracture path passing through different phases. The total length of the fracture path and the lengths through bright phase and dark phase (see Figure 37) can thus be obtained from these digitized coordinates. The measured length fractions of the fracture profiles (in %) obtained in this manner are reported in Table 9. The 'n' value represents the total number of field of views used to measure the length fractions in each of the specimens.

The digitized profile coordinate data were also used to obtain the linear fracture profile roughness parameter R_L and the profile structure factor Ψ from which the fracture surface roughness parameter Rs was estimated using Gokhale-Underwood equation given in Chapter II. As mentioned in Chapter II (also see equations 9 and 10) the surface roughness parameters are needed to compute the number of features per *unit true area of fracture surface* and true values of the mean dimple size on fracture surface from the measurements performed on the projected SEM images.

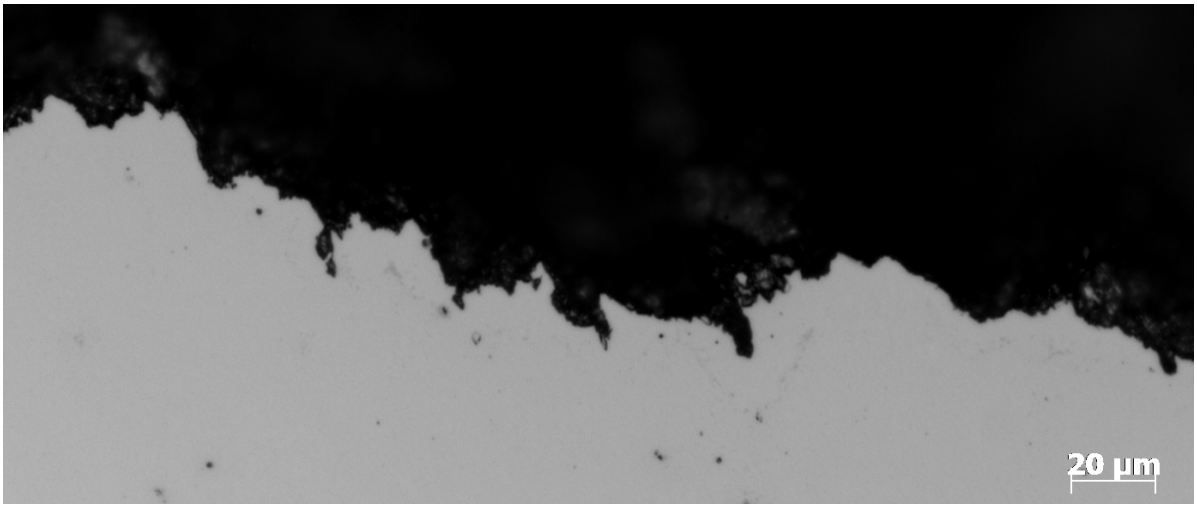

Figure 35: Shows the fracture profile in the unetched condition.

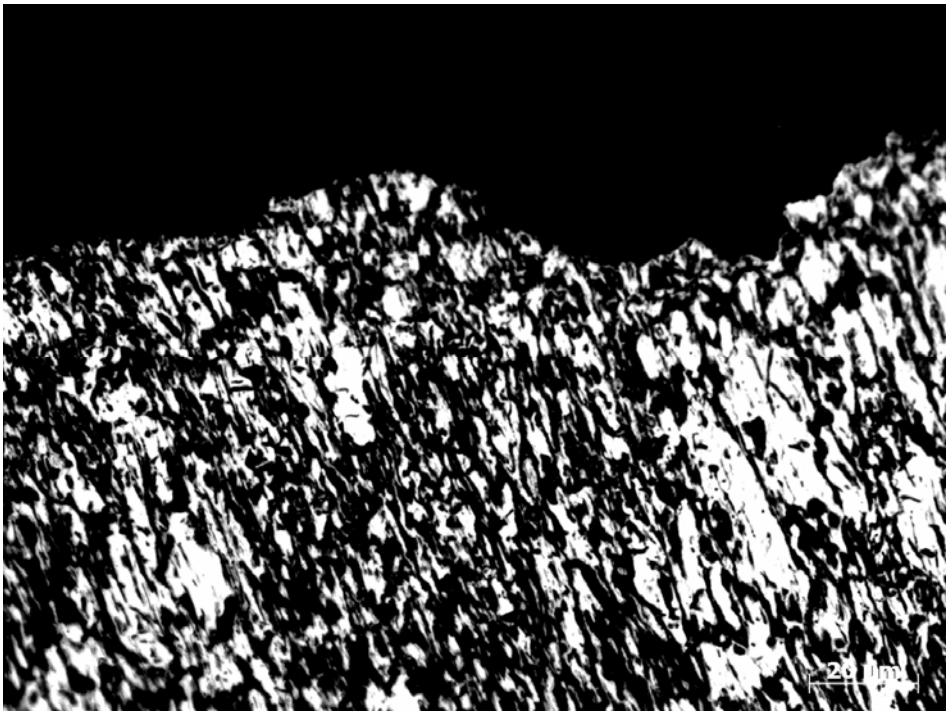

Figure 36: Shows the fracture path passing through white ferrite and black martensite.

Table 9

Measured value of the length fraction of the profile path (%) passing through the bright and dark regions of etched microstructure in the given set of dual phase steel samples.

Total Elongation (%)	Length profile passing through bright regions $L_{F\text{-measured}}$ (n= 21)	Length profile passing through dark regions $L_{M\text{-measured}}$ (n= 21)
10.1	68.25	31.75
11.9	65.09	34.91
13.1	65.9	34.1
14.0	66.0	34.0
15.8	66.27	33.73

The data in Table 9 gives the length fractions of the fracture profiles through bright and dark regions of the etched microstructures. It is important to point out that there are *three* possible paths from a fracture profile: (i) through the ferrite phase, (ii) through the martensite, and (iii) *along the interfaces between ferrite and martensite*. The segments of the fracture profile that go along the ferrite-martensite interfaces are measured as the profile segments through brightly etched regions or profile segments through the darkly etched regions with equal statistical probability because it purely depends on which half of the fractured specimen is being examined. The following figure clearly depicts how the measurements were made. The blue tracer path shows the fracture path through the darkly etched martensite phase while the red colored path shows the profile through the bright ferrite.

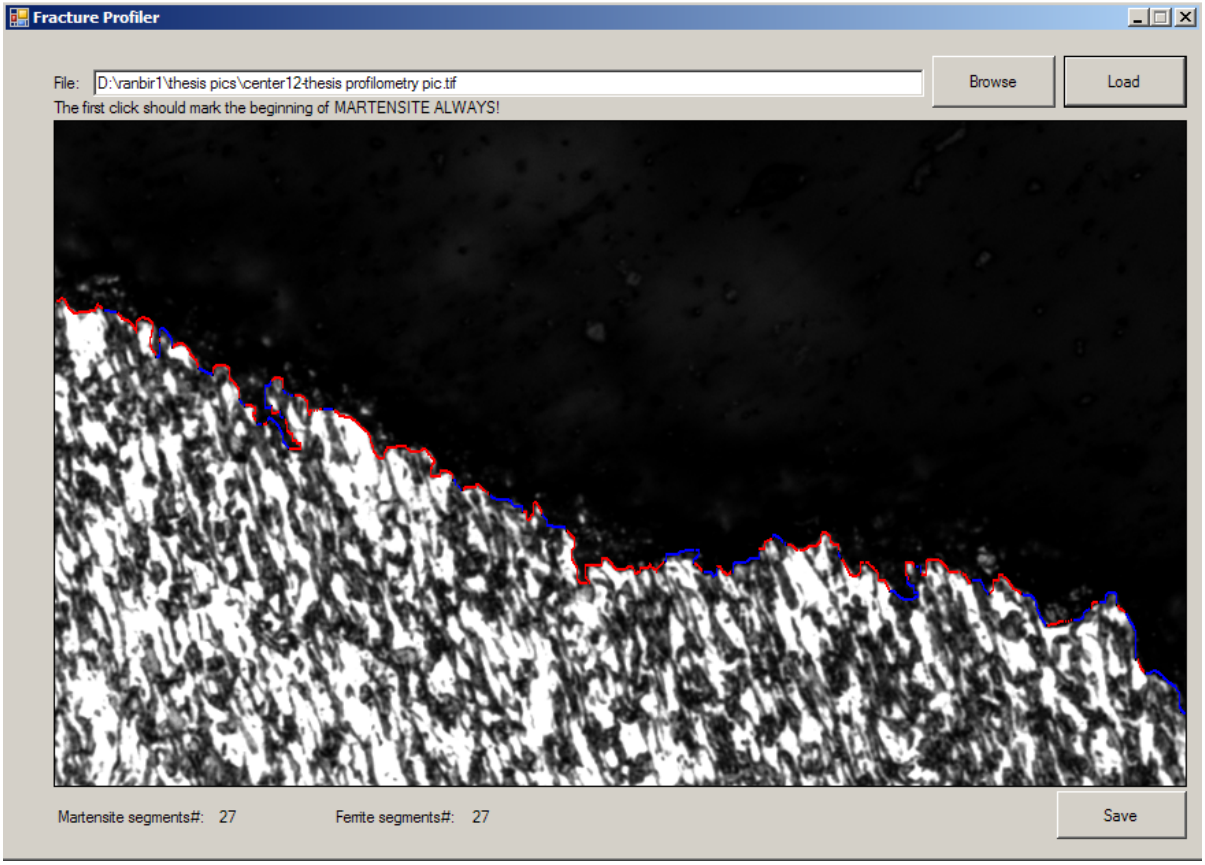

Figure 37: Shows the fracture path passing through white ferrite shown by the red tracer and black martensite shown by the blue tracer.

Therefore, just from these profilometric data it is not possible to uniquely determine the true fractions of fracture profile lengths through ferrite, martensite, and along the ferrite-martensite interfaces; additional information is needed for such estimations. The required additional information resides in the SEM fractographic data, and it is the area fraction through the ferrite-martensite interfaces, which is given in Table 6. From stereological principles, it can be shown that the length fraction of fracture profile along the ferrite-martensite interfaces is statistically equal to the area fraction of the fracture surface generated by decohesion of the ferrite-martensite interfaces as calculated from the

SEM images. These geometric arguments lead to the following equations for estimation of the length fractions of fracture profiles through the ferrite $(L_L)_{ferrite}$, through martensite $(L_L)_{martensite}$, and along the ferrite-martensite interfaces $(L_L)_{interface}$.

$$(L_L)_{interface} = (A_A)_{interface\text{-}SEM} \quad (19)$$

$$L_{F\text{-}measured} = (L_L)_{ferrite} + (1/2)\,(A_A)_{interface\text{-}SEM} \quad (20)$$

$$L_{M\text{-}measured} = (L_L)_{martensite} + (1/2)\,(A_A)_{interface\text{-}SEM} \quad (21)$$

In the above equations, $(A_A)_{interface\text{-}SEM}$ is the area fraction of the fracture surface generated by decohesion of ferrite-martensite interfaces measured through the SEM images (see Table 6), and $L_{F\text{-}measured}$ and $L_{M\text{-}measured}$ are obtained from the fracture profilometry data (Table 9). Therefore, using these equations the true length fractions of the fracture profiles through ferrite $(L_L)_{ferrite}$, through martensite $(L_L)_{martensite}$, and along ferrite-martensite interfaces $(L_L)_{interface}$ can be calculated. These parameters are reported in Table 10.

Table 10

True value of the length fraction of the profile path (%) passing through the ferrite and martensite phases in the given set of dual phase steel samples.

Total Elongation (%)	Length profile passing through ferrite $(L_L)_{ferrite}$	Length profile passing through martensite $(L_L)_{martensite}$	Length profile passing through ferrite-martensite interface $(L_L)_{interface\text{-}SEM}$
10.1	45.30+/- 1.56	8.80+/- 1.56	45.90 +/- 3.13
11.9	44.44+/- 2.13	14.26+/- 2.13	41.3+/- 4.27
13.1	50.10+/- 1.95	18.30+/- 1.95	31.60+/- 3.90
14	50.55+/- 1.30	18.55+/- 1.30	30.90+/- 2.60
15.8	52.17+/- 2.00	19.63+/- 2.00	28.20+/- 4.01

Inspection of Table 10 leads to the following important observations and conclusions.

- In all specimens, roughly half of the fracture profile (45 to 52%) goes through ferrite (see Figure 38 for visual comparison)
- In all specimens, less than 20% of the fracture profile goes through martensite although the global volume fraction of the martensite phase is around 60%. Therefore, it can be concluded that the fracture path tends to avoid going *through* martensite.

- There is a strong inverse correlation between the fraction of the fracture path along the ferrite-martensite interfaces $(L_L)_{interface}$ and the tensile ductility: $(L_L)_{interface}$ decreases systematically with the increase in the ductility.

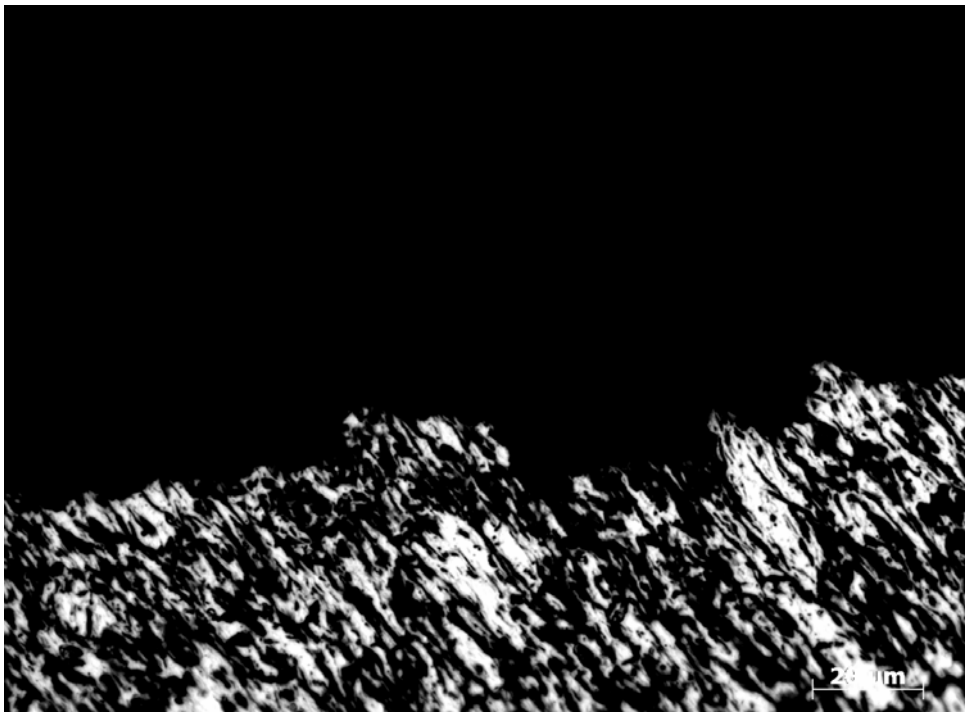

Figure 38: Shows the fracture path preferentially passing through the ferrite phase.

A more rigorous quantitative measure of the *affinity* of a phase with the fracture path can be obtained from the fracture affinity parameter Γ_i defined for i^{th} phase follows.

$$\Gamma_i = \{ [L_L]_i /([L_L]_i +[L_L]_j)\}/ [V_V]_I \quad (22)$$

$[L_L]_i$ is the fraction of fracture profile length through i^{th} phase (ferrite or martensite) and $[V_V]_i$ is the volume fraction of the i^{th} phase. The calculated values of the affinity parameters for ferrite and martensite phases are reported in Table 11. If the fracture path has a strong preference for a phase than Γ for that phase should be significantly higher

than one, and if the fracture path avoids a phase (repulsion) than Γ for that phase should be significantly less than one.

Table 11

Ratio of the true length fraction of the fracture profile passing through a particular phase and its bulk volume fraction for different specimens of dual phase steels.

Total Elongation (%)	$\Gamma_{ferrite}$	$\Gamma_{martensite}$
10.1	2.2	0.25
11.9	1.9	0.39
13.1	2.0	0.41
14.0	1.9	0.42
15.8	2.1	0.41

Inspection of Table 11 clearly reveals that the fracture path has a high affinity for ferrite and it tends to avoid martensite phase. In other words, martensite in this dual phase steel provides resistance to fracture, whereas ferrite facilitates the fracture process.

These trends may be explained on the basis of the chemical composition and heat treatment process subjected to the given grade of steels. Martensite is a hard phase as compared to ferrite and fracture taking place in dual phase steels due to martensite cracking or separation of the adjacent martensitic islands have been reported by many authors in the past. However for these set of samples as reported in table 4 the volume fraction of martensite is close to 60% making it the topologically continuous phase. With martensite being the major phase, with this increased volume fraction of martensite, the ferrite grains are more and more constrained by the surrounding martensite, which now

bears the initial macroscopic strain, which was initially taken by the softer ferrite phase only. This may be one of the reasons for the observed profilometry results.

As mentioned earlier, the chemistry of this dual phase steel is designed to increase the formability and weldability, which has profound influence on the fracture processes as well. The carbon content in these grades of dual phase steels has been lowered so as to circumvent the issues of formability and welding as a decrease in the %C content results in a corresponding decrease in the microhardness and hence increasing ductility. Thus with a decrease in the martensitic carbon content, a higher degree of deformation for martensite is achieved. With a balance of strength and ductility being imparted to the continuous phase of martensite, the ferrite in turn strain hardens less and this could be one of the reasons for the fracture path showing high affinity for the ferrite phase as revealed by the fracture affinity parameter Γ. Figure 12 shows the heat treatment given to the set of dual phase steel specimens. The heat treatment process involves tempering as the final stage, therefore the dual phase microstructure obtained contains tempered martensite. The fact that the martensite in these grades is tempered, could again be a possible cause of martensite not fracturing. Future work, relating the heat treatment parameters and the process conditions to the microstructural features should explicitly explain the fractography observations.

The tendency for decohesion between the two phases still remains one of the dominant failure mechanism as seen from the SEM fractography and fracture profilometry results. Though the martensite is imparted sufficient ductility by a lowered %C and by tempering, the non-uniformity in the strain distribution between the two phases still exists. This is evident seeing the SEM micrographs and the quantitative

results in Table 6, which indicate interface fracture taking place and resulting in huge packets of ferrite-martensite colonies being rooted out. The ferrite initially strain hardens with an increase in the dislocation density until the stress reaches the yield stress of martensite at the interface. This outcome of interface fracture basically occurs due to strain localization, which is attributed to the incompatible deformation between the two phases martensite and ferrite (which is softer of the two phases). It should be noted that decohesion tendency decreases from the lowest to the high ductility samples as shown in Table 10. This also corresponds to an increase in the fracture path passing through martensite. It clearly signifies that an increase in the deformation of martensite allows the fracture path to move transgranularly through it and hence prevent the interfacial fracture.

CHAPTER V

SUMMARY AND CONCLUSIONS

The thrust of this research is on understanding microstructural origins of the observed variability in the uniaxial tensile ductility of a set of cold rolled dual phase steel specimens having the same chemical composition and the same thermo-mechanical processing history. For this purpose, global representative microstructures and local microstructures in the vicinity of the fracture surfaces have been quantified using stereological techniques. In addition, the tensile fracture surfaces have been quantitatively characterized using SEM fractography and fracture profilometry. These experimental observations and quantitative data lead to the following important observations and conclusions.

- The representative global microstructures of all specimens are statistically similar. Therefore, the variability in the ductility is not due to the differences in the global microstructures of different specimens.
- In each specimen, the *local* microstructure just below the fracture surface *differs* from the corresponding global microstructure with respect to the morphological anisotropy of the ferrite-martensite interfaces and morphology of the ferrite regions. The severe local plastic deformation in the vicinity of the fracture surfaces leads to rotations of ferrite-martensite interfaces that cause the changes in the microstructural anisotropy. Rotations of the ferrite-martensite interfaces associated with the tendency to align along the direction of maximum shear stress, decreases the total projected area of these interfaces perpendicular to the applied tensile stress direction, and thereby, decreases the extent of the fracture path along ferrite-martensite interfaces.

- As the component of total ferrite-martensite interfacial area per unit volume in the local microstructure perpendicular to the applied tensile stress direction below the fracture surface *decreases,* the tensile ductility *increases* systematically. There is a strong inverse correlation between the magnitude of the component of ferrite-martensite total interfacial area perpendicular to the loading direction in the vicinity of the fracture surface and the tensile ductility. Consequently, the *variations in* the *local* ferrite-martensite total interfacial area perpendicular to the loading direction in the vicinity of the fracture surface is an important factor responsible for the observed variability in the ductility.

- The true number density of the pullouts of packets of ferrite-martensite colonies observed in the fracture surfaces is lower in the specimens having high tensile ductility. Likewise, fracture area fraction of the ferrite-martensite interface fracture is lower in the specimens having high tensile ductility.

- In all specimens, roughly half of the fracture profile (45 to 52%) goes through ferrite. In all specimens, less than 20% of the fracture profile goes through martensite although the global volume fraction of the martensite phase is around 60%. The fracture path has a high affinity for ferrite and it tends to avoid martensite phase. In other words, martensite in this dual phase steel provides resistance to fracture, whereas ferrite facilitates the fracture process. This may be attributed to the considerable amount of ductility being imparted to the topological continuous martensite phase by the chemical and thermomechanical processing of these dual phase steels.

- There is a strong inverse correlation between the fraction of the fracture profile path along the ferrite-martensite interfaces and the tensile ductility.

- Finally, the observed variability in the tensile ductility is due to *local variations* in the ferrite-martensite interfacial area and its anisotropy.

The present work on delineating the variability causes in the given set of dual phase steels specimens does not take into consideration the crystal orientation anisotropy which is important in the case of deformation of polycrystalline materials like in the present case. Void formation in these steels is dependent on the crystallographic relation between the neighboring ferrite and martensite grains. The variation in grain orientation does play a role in the gross macroscopic deformation behavior, which may be an additional influence on the cause of variability in the tensile ductility of these steels, apart from the factors discussed in this research work.

REFERENCES

[1] S. G. Tresvyatskii, "Dependence of the yield stress of metals on grain size," *Strength of Materials* ,vol. 3, No. 10, pp. 1320-1323, DOI: 10.1007/BF01530908.

[2] V.Y. Gertsman, M. Hoffmann, H. Gleiter and R. Birringer, "The study of grain size dependence of yield stress of copper for a wide grain size range," *Acta Metallurgica et Materialia*, vol. 42(10), pp. 3539-3544,1994.

[3] J. W. Aldrich and R. W. Armstrong , "The grain size dependence of the yield, flow and fracture stress of commercial purity silver," *Metall .Mat. Trans. B*, vol. 1, no.9, pp.2547-2550, DOI: 10.1007/BF03038382.

[4] George Dieter, "Mechanical Metallurgy", McGraw-Hill.

[5] A.M. Gokhale and G.R. Patel , "Quantitative fractographic analysis of variability in tensile ductility of a squeeze cast Al-Si-Mg base alloy," *Materials Charcterization*, vol. 54(1), pp. 13-20, 2005.

[6] S.G. Lee a, G.R. Patel , A.M. Gokhale , A. Sreeranganathan , M.F. Horstemeyer, "Quantitative fractographic analysis of variability in the tensile ductility of high-pressure die-cast AE44 Mg-alloy," Mater. Sci. Eng., vol.427, pp. 252-262, 2006.

[7] A.M. Sherman, and R.G. Daviesa, " Influence of martensite carbon content on the cyclic properties of dual-phase steel," *International Journal of Fatigue*, vol. 3(4), pp. 195-198, 1981.

[8] K.S. Choi, W.N. Liu, X. Sun and M.A. Khaleel, " Influence of Martensite Mechanical Properties on Failure Mode and Ductility of Dual-Phase Steels," *Metall .Mat. Trans.* A, vol.40A, pp.796-80, 2009.

[9] K.S. Choi, A. Soulami, W.N. Liu, M.A. Khaleel, X. Sun et al., "On key factors influencing ductile fractures of dual phase (DP) steels," *Materials Science and Engineering* A , vol. 526, pp.140–149, 2009.

[10] Peter Uggowitzer and Hein Peter Stiuwe,"The Tensile Fracture of Ferritic - Martensitic Carbon Steels," *Materials Science and Engineering*, vol. 55, pp.181 – 189, 1981.

[11] R.T. DeHoff and F.N. Rhines, " Quantitative Microscopy", McGraw-Hill, New York. NY, 1968.

[12] E.E.Underwood, " Quantitative Stereology", Addison-Wesley, Reading, Mass.,1970.

[13] A.M. Gokhale, “Quantitative fractography”, ASM Handbook, vol. 11, pp.538-556, 2002.

[14] A.M. Gokhale, W.J.Drury, and S.Mishra, “ Recent Developments in Quantitative fractography”,ASTM STP 1203, pp.3-22,1993.

[15] N.U. Deshpande, A.M. Gokhale, D.K. Denzer, and John Liu, “Relationship Between Fracture Toughness, Fracture Path, and Microstructure of 7050 Aluminium Alloy -1: Quantitative Characterization”, *Metall. Mat.Trans*., vol.29A, pp.1191-1201,1988.

[16] G.E. Pellissier, “Effects of Microstructure on the Fracture Toughness of Ultra High Strength Steels,” *Engineering Fracture Mechanics*, Vol.1, pp.55-75, 1968.

[17] N. Saeidi, A. Ekrami , “Comparison of mechanical properties of martensite/ferrite and bainite/ferrite dual phase 4340 steels,” *Materials Science and Engineering* A, vol.523, pp.125–129, 2009.

[18] V. Colla, M. De Sanctis, A. Dimatteo, G. Lovicu, A. Solina, and R. Valentini, “Strain Hardening Behavior of Dual-Phase Steels,” *Metall. Mat.Trans A*., vol. 40A, p.2557, 2009.

[19] Takehide Senuma, “Physical Metallurgy of Modern High strength steels,” *Int. J. Plasticity*, vol.41, no. 6, pp. 520-532, 2001.

[20] A.Murgaiyan, R.R.Mohanty, Ashwin Pandit, Arjit Saha Podder, N Gope, “Effect of composition on microstructure and mechanical properties of dual phase steels- a Review”.

[21] M. MAZINANI and W.J. POOLE, “Effect of Martensite Plasticity on the Deformation Behavior of a Low-Carbon Dual-Phase Steel,” *Metall. Mat.Trans A*,vol. 38A, p.328 , 2007.

[22] K. S. Choi, W. N. Liu, X. Sun, M. A. Khaleel, J. R. Fekete, “Influence of Manufacturing Processes and Microstructures on the Performance and Manufacturability of Advanced High Strength Steels,” *Journal of Engineering Materials and Technology*, vol. 131, 2009.

[23] Süleyman Gündüz, “Effect of chemical composition, martensite volume fraction and tempering on tensile behaviour of dual phase steels,” *Materials Letters* 63, pp.2381–2383, 2009.

[24] G.Caballero, Andrea Garcia-Juneeda, Carlos Capdevila,Carlos Garcia de Andres, “Evolution of Microstructural Banding during the Manufacturing Process of Dual Phase Steels,” *Materials Transactions*, vol.47,no.9,pp.2269-2276, 2006.

[25] G.Avramovic-Cingara, Ch.A.R.Saleh, M.K.Jain and D.S.Wilkinson, "Void Nucleation and Growth in Dual-Phase Steel 600 during Uniaxial Tensile Testing," *Metall. Mat.Trans A*, vol.40A,pp. 3117-3127, 2009.

[26] Mehmet Erdogan, Suleyman Tekeli, "The effect of martensite particle size on tensile fracture of surfacecarburised, AISI 8620 steel with dual phase core microstructure," *Materials and Design*, vol. 23, pp.597-604, 2002.

[27] G. Avramovic-Cingaraa, Y. Ososkova, M.K. Jain b, D.S. Wilkinsona, "Effect of martensite distribution on damage behaviour in DP600 dual phase steels," *Metall. Mat.Trans A*, vol. 516, pp. 7-16, 2009.

[28] H. P. Shen, T. C. Lei, J. Z. Liu, " Microscopic deformation behaviour of martensitic ferritic dual-phase steels," *Materials Science and Technology* , vol. 2, p. 28, 1986.

[29] C.C.Tasan, J.P.M.Hoefnagels and M.G.D. Geers, " Microstructural banding effects clarified through micrographic digital image correlation," *Scripta Materialia* , vol.62, pp.835-83, 2010.

[30] M.Mazinani, W.J.Poole, Adv.Mater. Res.15-17(2007) 774.

[31] A.N.Bortsov, N.M.Fonshteyn, *Phys.Met.Metall*. 61 (2)(1986) 74

[32] X.J.He,N.Terao, A.Berghezan, *Metal Sci.* 18 (1984) 367.

[33] N.J.Kim,G.thomas, *Metall.Trans*. 12A(1981) 483.

[34] J.Lian, Z.Jiang, and J. Liu, *Mater. Sci. Eng*.,vol. A 147, pp. 55-65, 1991.

[35] X. Sun , K.S. Choi, W.N. Liu, M.A. Khaleel, "Predicting failure modes and ductility of dual phase steels using plastic strain localization," *International Journal of Plasticity*, vol.25, pp.1888–1909, 2005.

[36] E. Maire a,*, O. Bouaziz b, M. Di Michiel c, C. Verdu, "Initiation and growth of damage in a dual-phase steel observed by X-ray microtomography," *Acta Materialia*, vol. 56, pp. 4954–4964, 2008.

[37] A.J. Baddeley, H.J. Gundersen and L.M. Cruz-Orive, *Journal of Microscopy*, vol.142 , pp. 259-276, 1986.

[38] A.M. Gokhale and W.J. Drury, *Metall. Mat.Trans A*, vol. 25A, pp.919-929, 1994.

[39] P. B. Corson, "Correlation functions for predicting properties of heterogeneous Materials-Experimental measurement of spatial correlation functions in multiphase solids," *J. Appl. Phy.s*, vol. 45, no. 7, pp. 3159-3164, 1974/7, 1974.

[40] H. L. Frisch, and F. H. Stillinger, "Contribution to the statistical geometric basis of radiation scattering," *Journal of Chemical Physics*, vol. 38, no. 9, pp. 2207, 1963.

[41] P. Louis and A.M. Gokhale, Metall. Trans. A, 1995, vol.26 A, pp.1449-1454.

[42] A.M.Gokhale, and E.E. Underwood, " A General Method for Estimation of Fracture Surface Roughness, Part I", *Metallurgical Transaction A*, vol. 21A 1990, pp.1191-1199.

[43] A.M.Gokhale, and E.E. Underwood, " A General Method for Estimation of Fracture Surface Roughness, Part II", *Metallurgical Transaction A*, vol. 21A 1990, pp.1201-1207.

[44] H.Agrawal, A.M.Gokhale, S.Graham, M.F. Horstemeyer, D.J. Bamman, " Rotations of brittle particles during plastic deformation of ductile alloys," *Materials Science and Technology* , vol. 328A, pp. 310-316, 2002.